



1 The pan-tropical response of soil moisture to El Niño

2 Kurt C. Solander¹, Brent D. Newman¹, Alessandro Carioca de Araujo², Holly R. Barnard³, Z. Carter
3 Berry⁴, Damien Bonal⁵, Mario Bretfeld^{6,13}, Benoit Burban⁷, Luiz Antonio Candido⁸, Rolando Céleri⁹,
4 Jeffery Q. Chambers¹⁰, Bradley O. Christoffersen¹¹, Matteo Detto^{12,13}, Wouter A. Dorigo¹⁴, Brent E.
5 Ewers¹⁵, Savio José Filgueiras Ferreira⁸, Alexander Knohl¹⁶, L. Ruby Leung¹⁷, Nate G. McDowell¹⁷,
6 Gretchen R. Miller¹⁸, Maria Terezinha Ferreira Monteiro¹⁹, Georgianne W. Moore²⁰, Robinson
7 Negron-Juarez¹⁰, Scott R. Saleska²¹, Christian Stiegler¹⁶, Javier Tomasella²², Chonggang Xu¹

8
9 ¹ Earth and Environmental Sciences, Los Alamos National Laboratory, Los Alamos, NM

10 ² Brazilian Agricultural Research Corporation, Embrapa Amazônia Oriental, Manaus, Brazil

11 ³ Department of Geography, University of Colorado, Boulder, CO

12 ⁴ Schmid College of Science and Technology, Chapman University, Orange, CA

13 ⁵ Université de Lorraine, AgroParisTech, INRA, UMR Silva F-54000, Nancy, France

14 ⁶ Department of Ecology, Evolution, and Organismal Biology, Kennesaw State University, Kennesaw,
15 GA

16 ⁷ INRA, UMR EcoFoG, AgroParisTech, Cirad, CNRS, Université des Antilles, Université de Guyane,
17 Kourou, France

18 ⁸ Coordination of Environmental Dynamics, National Institute for Amazonia Research, Manaus,
19 Brazil

20 ⁹ Department of Water Resources and Environmental Sciences, University of Cuenca, Cuenca,
21 Ecuador

22 ¹⁰ Earth and Environmental Sciences, Lawrence Berkeley National Laboratory, Berkeley, CA

23 ¹¹ Department of Biology, University of Texas Rio Grande Valley, Edinburg, TX

24 ¹² Department of Ecology and Evolutionary Biology, Princeton University, Princeton, NJ

25 ¹³ Smithsonian Tropical Research Institute, Panama City, Panama

26 ¹⁴ Department of Geodesy and Geoinformation, Vienna University of Technology, Vienna, Austria

27 ¹⁵ Department of Botany, University of Wyoming, Laramie, WY

28 ¹⁶ Bioclimatology, University of Goettingen, Goettingen, Germany

29 ¹⁷ Atmospheric Sciences and Global Change, Pacific Northwest National Laboratory, Richland, WA

30 ¹⁸ Civil Engineering, Texas A&M University, College Station, TX

31 ¹⁹ Climate and Environment, National Institute for Amazonia Research, Manaus, Brazil

32 ²⁰ Department of Ecosystem Science and Management, Texas A&M University, College Station, TX

33 ²¹ Ecology and Evolutionary Biology, University of Arizona, Tucson, AZ

34 ²² Coordination of Research and Development, National Centre for Monitoring and Early Warning of
35 Natural Disasters, Cachoeira Paulista, Brazil

36

37

38

39

40

41

42

43

44

45

46

47

48



49 **Abstract**

50 The 2015-16 El Niño event ranks as one of the most severe on record in terms of the
51 magnitude and extent of sea surface temperature (SST) anomalies generated in the tropical
52 Pacific Ocean. Corresponding global impacts on the climate were expected to rival, or even
53 surpass, those of the 1997-98 severe El Niño event, which had SST anomalies that were
54 similar in size. However, the 2015-16 event failed to meet expectations for hydrologic change
55 in many areas, including those expected to receive well above normal precipitation. To better
56 understand how climate anomalies during an El Niño event impact soil moisture, we
57 investigate changes in soil moisture in the humid tropics (between $\pm 25^\circ$) during the three
58 most recent super El Niño events of 1982-83, 1997-98, and 2015-16, using data from the
59 Global Land Data Assimilation System (GLDAS). First, we validate the soil moisture estimates
60 from GLDAS through comparison with in-situ observations obtained from 16 sites across five
61 continents, showing an r^2 of 0.54. Next, we apply a k-means cluster analysis to the soil
62 moisture estimates during the El Niño mature phase, resulting in four groups of clustered
63 data. The strongest and most consistent decreases in soil moisture occur in the Amazon basin
64 and maritime southeast Asia, while the most consistent increases occur over east Africa. In
65 addition, we compare changes in soil moisture to both precipitation and evapotranspiration,
66 which showed a lack of agreement in the direction of change between these variables and
67 soil moisture most prominently in the southern Amazon basin, Sahel and mainland southeast
68 Asia. Our results can be used to improve estimates of spatiotemporal differences in El Niño
69 impacts on soil moisture in tropical hydrology and ecosystem models at multiple scales.

70

71



72 **Introduction**

73 The El Niño Southern Oscillation (ENSO) is one of the major coupled ocean-
74 atmosphere modes of variability internal to the Earth system operating on interannual
75 timescales (Jones et al., 2001). ENSO refers to basin-wide changes in the air-sea interaction
76 associated with changes in the sea surface temperatures (SSTs) of the tropical Pacific region.
77 Depending on the directionally of the SST deviation, ENSO events are classified in two
78 modes—El Niño, or the warm mode, when unusually warm water exists in the eastern
79 tropical Pacific Ocean off the South American coast—and La Niña, or the cool mode, when
80 anomalously cool water pools exist in approximately the same location (Trenberth, 1997).
81 Associated impacts on weather and climate over terrestrial areas are variable but typically
82 strongest in the low-latitude and some of the mid-latitude regions of North and South
83 America, east Africa, Asia and Australia (Ropelewski and Halpert, 1989); however, the
84 influence of ENSO on weather and climate has been detected around the globe outside of
85 these regions through teleconnection (Iizumi et al., 2013). Although we bring up ENSO here
86 to highlight the mode duality of this climate feature, the focus of our study presented here is
87 solely on the El Niño mode of ENSO.

88 An important factor that controls the teleconnection in climate and weather patterns
89 caused by El Niño is the magnitude of the given El Niño event. Of the 39 El Niño events that
90 have occurred since 1952, those occurring in 1972-73, 1982-83, 1997-98 and 2015-16 are
91 categorized as “super El Niño” events (Hong et al., 2014). Although occurring at a much
92 lower frequency than a non-super El Niño event, these events account for a
93 disproportionately large amount of the global climate anomalies associated with El Niño.
94 There is debate as to whether or not the 2015-16 event can be classified as a super El Niño



95 based on the lack of specific features that characterize a super El Niño including strong far
96 east Pacific SST anomalies, unusually high global SSTs, reduced outgoing longwave radiation
97 (OLR), and weaker surface wind and sea surface height in the eastern Pacific (Hameed et al.,
98 2018). We use the definition put forth by Hong et al., (2014) that defines a super El Niño as
99 one with Niño-3 SST anomalies greater than one standard deviation above others in the
100 instrumental record (Trenberth, 1997), coupled with a Southern Hemispheric transverse
101 circulation that is robust relative to that of other El Niños. The 2015-16 event fits the super
102 El Niño classification using this definition (Huang et al., 2016; Chen et al., 2017).

103 Prediction of the climatic or hydrologic response over the land surface from an El
104 Niño has proved to be difficult even during a super El Niño event. For example, none of the
105 25 forecasts of precipitation patterns produced from various models could accurately
106 predict precipitation over the western US during the 2015-16 El Niño event (Wanders et al.,
107 2017). Indeed, Wanders et al., (2017) reported that less than half of the forecasts predicted
108 the directionality of precipitation changes correctly. An evaluation of the three most recent
109 super El Niños revealed that although drought during January to March (JFM) was
110 widespread over the entire Amazon basin during the 1982-83 and 1997-98 events, during
111 the 2015-16 event the western half of the basin actually got wetter (Jiménez-Muñoz et al.,
112 2016). The authors indicate that spatial differences in the SST anomaly during JFM 2015-16
113 relative to other super El Niños may have contributed to this anomaly (e.g. Yu and Zou,
114 2013).

115 Given the diversity of El Niño impacts on precipitation, it is not clear how land surface
116 hydrology at a global scale may be influenced by El Niño and whether such an influence may
117 be more region-specific even in tropical areas that are close to the El Niño source region



118 where impacts are generally expected to be more pronounced (Schubert et al., 2016). This
119 lack of understanding is reflected in substantial multi-spatial and temporal scale errors in
120 ENSO impacts on hydrology in models (Zhuo, et al., 2016). Of the land surface hydrologic
121 variables, soil moisture is of particular interest due to the scarcity of observations available
122 to properly evaluate its response to El Niño (Gruber et al., 2018), particularly in the low
123 latitude tropics (Dorigo et al., 2011), as opposed to the more well-studied response of
124 precipitation over the same region (Ropelewski and Halpert, 1989; Dai and Wigley, 2000;
125 Chou et al., 2009; Huang and Chen, 2017; Xu 2017). Moreover, understanding soil moisture
126 variability to macroclimatic events is useful because of its role in partitioning the energy
127 fluxes at the Earth's surface (Seneviratne et al., 2010), as well as its importance as a driver
128 of tropical biomass productivity (Raddatz et al., 2007) and ecosystem responses within Earth
129 System Models (ESMs) (Green et al., 2019).

130 Several additional factors highlighted in previous studies contribute to the
131 uncertainty of how soil moisture will respond to El Niño for different areas. A study in which
132 soil moisture anomalies were regressed against the Southern Oscillation Index (SOI), one of
133 the indices of ENSO intensity, revealed that within the tropics, soil moisture typically
134 decreases during El Niño events, with notable exceptions occurring in extreme southern
135 Africa and parts of South America (Miralles et al., 2014). However, much of the data used in
136 the analysis from the tropics were actually missing because they were derived from active
137 and passive microwave satellite sensors that fail to penetrate the ground beneath dense
138 rainforests, resulting in substantial data gaps throughout the tropical regions (Liu et al.,
139 2012; Dorigo et al., 2017). Another study used a coupled biosphere-hydrology model
140 simulation and determined that soil moisture decreased in the Amazon basin during the



141 2015-16 super El Niño with more acute reductions occurring in the northeastern part of the
142 basin (van Schaik et al., 2018). Given that the study did not assess changes over the region
143 during other super El Niño events, it is unclear if a similar spatial pattern emerges during El
144 Niños that are comparable in magnitude.

145 Building on these previous studies, we evaluate the soil moisture response to El Niño
146 within the humid tropics from 1979 to 2016 with a focus on three super El Niño events. We
147 concentrate our assessment on soil moisture because of its strong controls on energy and
148 water exchanges at the land-atmosphere interface and because it represents the main source
149 of water for natural and cultivated vegetation (Prigent et al., 2005). Soil moisture data for
150 the analysis was derived from the monthly Global Land Data Assimilation System (GLDAS)
151 products at one-degree resolution, which are spatially continuous across the globe since
152 January 1979 (Rodell et al., 2004). The continuous temporal resolution of this data product
153 satisfies one of our goals by enabling evaluation of the soil moisture response across the
154 three super El Niños: 1982-83, 1997-98 and 2015-16, which has never before been done.
155 The continuous spatial coverage of GLDAS enables analysis of the soil moisture response
156 across all tropical regions, including dense rainforests, which was limited to less densely
157 forested areas in studies reliant on remote sensing (e.g. Miralles et al., 2014).

158

159 **Methods**

160 GLDAS data was downloaded from the Giovanni online data system, which is
161 maintained by the National Aeronautics and Space Administration Goddard Earth Sciences
162 Data and Information Services Center (NASA GES DISC, Acker and Leptoukh, 2007). Data
163 from GLDAS is derived from precipitation gauge records, satellite data, radar precipitation



164 observations and various outputs from numerical models (Rodell et al., 2004). We used
165 1979-2016 monthly data from all four GLDAS land surface models (LSMs) including the
166 Variable Infiltration Capacity (VIC) model (Liang et al., 1994), Community Land Model (CLM)
167 (Dai et al., 2003), Noah LSM (NOAH) (Ek et al., 2003) and the Mosaic LSM (MOSAIC) (Koster
168 and Suarez, 1996). GLDAS soil moisture data is used as the basis for this analysis because
169 soil moisture estimates from the four individual GLDAS LSMs capture the range of variability
170 in other similar global soil moisture data products at the locations of the in-situ data that was
171 used in this study and described in Table 1 (Fig. 1). Other data products in this comparison
172 include the fifth generation European Center for Medium-Range Weather Forecasts
173 (ECMWF) reanalysis soil moisture product (ERA5) (Copernicus Climate Change Service
174 (C3S), 2017), the Modern-Era Retrospective analysis for Research and Applications, Version
175 2 (MERRA2) (Gelaro et al., 2017) and the Global Land Evaporation Amsterdam Model
176 (GLEAM) (Miralles et al., 2011; Martens et al., 2017). All three datasets have a spatial
177 resolution of 0.25°. To avoid integration of results from different climate zones, which are
178 likely to show a dissimilar soil moisture response, we targeted only GLDAS pixels considered
179 to be part of the humid tropics by creating a mask using data from the Köppen-Geiger climate
180 classification system (Kottek et al., 2006) obtained from the Spatial Data Access Tool (SDAT)
181 (ORNL DAAC, 2017a). The mask was used in conjunction with the monthly soil moisture
182 estimates to isolate changes specific to the tropical climate zone.

183 In addition to the four data products mentioned above, we also considered using the
184 European Space Agency Climate Change Initiative (ESA CCI) global soil moisture product
185 (Dorigo et al., 2017). However, because this product is derived from observations from
186 satellite microwave sensors that have difficulty retrieving data beneath dense rainforest



187 canopies, ESA CCI soil moisture estimates within the tropics were too sparse to reliably
188 determine the spatially continuous soil moisture response to El Niño across all tropical
189 regions (e.g. Liu et al., 2012).

190 Soil moisture is represented in each of the four GLDAS LSMs in a sequence of
191 subsurface layers up to a maximum of three to ten layers. Each subsurface layer represented
192 in GLDAS varies in depth up to an aggregated, multi-layer maximum depth of 3.5 m among
193 the four models. We only used data from the uppermost group of soil layers within each
194 model closest to a depth of 0-10 cm. This was done to target the near-surface soil moisture
195 response to El Niño, as the El Niño signature in soil moisture at shallow depths is likely to be
196 more prominent and the largest number of in-situ observations that are available for
197 comparison to the GLDAS estimates also come from the near surface zone. We used the
198 ensemble mean at 0-10 cm depth from the four models because the ensemble is considered
199 to provide a more robust representation of reality (Tebaldi and Knutti, 2007).

200 Soil moisture estimates from GLDAS were validated through comparison to in-situ
201 observations across 16 sites spanning five continents (Table 1). These data were accessed
202 through a variety of sources including the Cosmic-ray Soil Moisture Observing System
203 (COSMOS) (Köhli et al., 2015), United States Department of Agriculture Soil Climate Analysis
204 Network (SCAN) (Schaefer et al., 2007), Plate Boundary Observatory (PBO) (Larson et al.,
205 2008), International Soil Moisture Network (ISMN) (Dorigo et al., 2011; Dorigo et al., 2013),
206 several FLUXNET sites (Goulden et al., 2004; Beringer et al., 2007; Bonal et al., 2008; Beringer
207 et al., 2011; Beringer et al., 2013) and other individual data collaborators who have made
208 their data available for use in this study. Data from the individual GLDAS LSMs were
209 interpolated to the same depths as the in-situ data shown in Table 1 using cubic spline and



210 linear interpolation prior to ensemble averaging and comparison with the in-situ data. When
211 interpolating data from CLM, which includes soil moisture estimates for ten distinct
212 subsurface layers, cubic spline interpolation was used. Linear interpolation was used for the
213 other three GLDAS models, which include soil moisture estimates from either three or four
214 distinct subsurface layers where cubic spline interpolation would have been less
215 appropriate. The GLDAS data was compared to in-situ data using the linear relationship
216 shown in Equation 1:

217

$$218 \quad SM_I = \beta_0 + \beta_1 * SM_G \quad (1)$$

219

220 where SM_I is the in-situ soil moisture observation (%), β_0 is the y-intercept (%), β_1 is the
221 slope and SM_G is the GLDAS ensemble soil moisture estimate (%). The coefficients of the
222 linear relationship in Equation 1 were used to provide a bias-corrected estimate of soil
223 moisture from GLDAS that was more representative of the near-surface in-situ soil moisture
224 observations. The bias-corrected estimates are compared to in-situ observations to assess
225 how application of the bias-correction method improves the representation of soil moisture
226 at the point scale.

227 In-situ soil moisture observations were compared to corresponding GLDAS soil
228 moisture estimates at co-located depths for pixels that encompassed the in-situ observation.
229 In some situations, adjacent pixels were used if data from the co-located GLDAS pixel was
230 missing, e.g., over lands adjacent to inland water bodies or oceans, due to the coarse
231 resolution of the GLDAS dataset. The same data comparison was made after removing data
232 from one site in Ecuador and another from Australia. In-situ observations from these sites



233 were not likely to be representative of the GLDAS data at one-degree resolution given that
234 the sites where data was collected are either located at a high elevation of 3,780 m or
235 seasonally flooded wetland where the sub-surface soil is frequently saturated. Observations
236 from one site in Brazil were also removed due to poor agreement between observations and
237 GLDAS data relative to other sites.

238 Comparison of soil moisture from GLDAS to in-situ point-based measurements does
239 have an inherent scale mismatch. For example, measurements at an individual site may not
240 necessarily represent soil moisture conditions at the scale of a GLDAS pixel due to
241 heterogeneities in land cover, soil or topography. However, given the previously noted
242 challenges regarding the dearth of large-scale moisture measurements in the tropics, the
243 site-based data represent the best available source of actual soil moisture contents in this
244 region. Scale mismatch effects are also moderated by use of multiple sites spanning multiple
245 continents. Site-based measurements of soil moisture considered to be outliers in terms of
246 how they compare to the co-located GLDAS pixel soil moisture estimate are examined further
247 in the discussion section.

248 The soil moisture response to El Niño for the three super El Niño events of 1982-83,
249 1997-98 and 2015-16 was calculated by taking the difference in the GLDAS soil moisture
250 during the El Niño mature phase of October to December (OND) and January to March (JFM)
251 from the long-term 1979-2016 climatological monthly mean (Eqs. 2 and 3):

252

$$253 \quad \Delta SM_{OND} = SM_{OND} - \sum_1^n SM * n^{-1} \quad (2)$$

$$254 \quad \Delta SM_{JFM} = SM_{JFM} - \sum_1^n SM * n^{-1} \quad (3)$$

255



256 where SM is the 3-month mean GLDAS soil moisture during the mature phase (either OND
257 or JFM) of the focal year for three super El Niños (1982-83, 1997-98 and 2015-16) and n
258 indicates the total number of monthly estimates used in the analysis from 1979-2016.

259 K-means cluster analysis was used to determine groups of pixels representing soil
260 moisture anomaly with a similar magnitude and direction of change during OND and JFM
261 across the three super El Niño events. Clustering was based on the ΔSM for OND and JFM
262 that were calculated using Equations 2 and 3. Prior to conducting the analysis, the ΔSM
263 values were re-scaled to have a mean of 0 and standard deviation of 1. The mean and
264 standard deviation of OND and JFM ΔSM within each clustered region was then used to
265 assess the consistency of soil moisture response for different clustered regions.

266 The number of clusters used in the K-means cluster analysis was set to four. This
267 number was selected based on results from a suite of tests used to determine the optimal
268 number of clusters using the R package NbClust (version 3.0) (Charrad et al., 2014). Each
269 test uses a set of criteria to generate a score for the proposed number of clusters (ranged
270 between four and ten). We used only tests where the optimal number of clusters was based
271 on which proposed number of clusters had the maximum or minimum score so the proposed
272 cluster groups could be ranked accordingly. The mean ranking for all tests across all periods
273 (OND and JFM for three super El Niños) was then used to determine the optimal number of
274 clusters (Table 2).

275 The response of precipitation and evapotranspiration (also obtained from GLDAS) to
276 El Niño was also determined to compare against the soil moisture responses. The
277 precipitation and evapotranspiration responses (ΔP and ΔET) to the three super El Niños
278 are calculated following the same metric for the soil moisture responses (ΔSM) shown in



279 Equations 2 & 3. The OND and JFM ΔSM is compared to ΔP and ΔET for the three super El
280 Niños and plotted on maps as the $\Delta SM:\Delta P$ and $\Delta SM:\Delta ET$ ratios. The pixel-wide mean $\Delta SM:\Delta P$
281 and $\Delta SM:\Delta ET$ ratios and standard deviations for each of the four clustered regions during
282 OND and JFM are also summarized.

283 The relationship between soil moisture and El Niño is further evaluated by calculating
284 the Pearson correlation coefficient (r) between the 1979-2016 GLDAS monthly soil moisture
285 and the monthly Niño-3.4 index (Trenberth, 1997; Bunge and Clarke, 2009) for all GLDAS
286 pixels in the humid tropics. The Niño-3.4 index is a variant of the Niño-3 index region in that
287 it is centered further west ($120 - 170^\circ W$ vs $90 - 150^\circ W$) at the same latitude range ($5^\circ N -$
288 $5^\circ S$). The Niño-3.4 index data was downloaded from the NOAA/OAR/ESRL PSD, Boulder,
289 Colorado web site at <http://www.esrl.noaa.gov/psd> (accessed 24 October 2017). The mean
290 correlation was calculated and summarized for the same regions that were derived from the
291 cluster analysis. The same correlation analysis was conducted using the soil moisture
292 response lagged by up to six months for the four clustered regions during OND and JFM.
293 Because this failed to increase the amount of variability in soil moisture estimates that could
294 be explained by Niño-3.4 over any of the clustered regions by more than 1%, we only present
295 correlation results with no lag.

296 Finally, we calculated the soil moisture response to El Niño for the tropics using the
297 bias-corrected estimates of GLDAS soil moisture that were derived from the comparisons
298 with the in-situ soil moisture data. We compare this to the unbiased estimates to determine
299 the spatial variability in the magnitude of mismatch between these two estimates. Given the
300 limited number of in-situ observations that were available to generate the bias-corrected
301 estimates, we use this only to highlight regions where a higher density of soil moisture



302 observations might be necessary to improve the accuracy of the soil moisture response to El
303 Niño derived from GLDAS.

304

305 **Results**

306 GLDAS soil moisture estimates were validated against all in-situ soil moisture
307 estimates as well as through the removal of three outliers (Fig. 2). Exclusion of the Ecuador,
308 Australia and Brazil data resulted in an overall reduction in the number of observations by
309 15% but dramatic improvement in the r^2 between GLDAS and in-situ estimates from 0.03 to
310 0.54. Comparison of these datasets following the removal of outliers reveals a consistent
311 positive bias in the GLDAS soil moisture estimates relative to in-situ observations.
312 Consequently, the equation from the best-fit linear regression line (Eq. 1) was used to reduce
313 the bias in the GLDAS estimates (Fig. 2). Use of the bias-corrected soil moisture estimates
314 from GLDAS resulted in a mean reduction of RMSE across all sites by 69% (Fig. 3). The
315 resulting RMSE and r^2 coefficient of determination across these sites ranged from 0.03-0.24
316 (mean = 0.08) and 0.00 to 0.88 (mean = 0.45), respectively (Fig. 4).

317 Our results of soil moisture changes over regions derived from the cluster analysis
318 show that the most consistent and strongest decreases in OND soil moisture during the three
319 super El Niño events occurred over the northeast Amazon Basin and maritime southeast Asia
320 (Fig. 5a). Regions with the largest and most consistent increases in OND soil moisture over
321 the three events include eastern and southern equatorial Africa, Latin America and southern
322 India. Notably, the positive anomalies are much larger during 1982 and 1997 than in 2016.
323 During the late mature phase of El Niño (JFM), the strongest and most consistent decreases
324 in soil moisture during the three super El Niño events were centered north of the equator,



325 while consistent increases largely occurred south of the equator (Fig. 5b). This pattern holds
326 more or less consistent across the three major land masses of South America, Africa and
327 Asia/Australia. The largest overall increase in soil moisture was centered over the southern
328 Amazon Basin. Similar to the changes observed during OND, the positive anomalies tended
329 to be larger during the two earlier El Niños of 1983 and 1998.

330 Four clusters are shown for each of the OND (Fig. 6a) and JFM (Fig 6b) periods. The
331 cluster with the highest soil moisture increases is Cluster-3 followed by Cluster-4, while the
332 highest soil moisture decreases are found in Cluster-2 followed by Cluster-1. The cluster
333 results during OND confirm the locations of the largest, most consistent soil moisture decreases
334 (denoted by Cluster-2) over the northeast Amazon Basin and increases (denoted by Cluster-
335 3) over east Africa, Latin America and southern India (Fig. 6a). The mean decrease in soil
336 moisture over the Cluster-2 region during OND varied between -0.06 to -0.15 over the three
337 super El Niño events, while the mean increase in soil moisture over the Cluster-3 region
338 varied between 0.04 to 0.06 (Table 3). Similarly, during JFM the cluster results show
339 decreases centered north of the equator and increases south of the equator with smaller
340 overall coverage of Cluster-3 occurring in 2016 (Fig. 6b). The cluster results during JFM
341 confirm the locations of the largest, most consistent soil moisture decreases (denoted by
342 Cluster-2) over the northeast Amazon Basin and increases (denoted by Cluster-3) over east
343 Africa, Latin America and southern India (Fig. 6b). The mean decrease in the Cluster-2 region
344 during JFM varied between -0.10 to -0.12 over the three super El Niño events, while the mean
345 increase in Cluster-3 varied between 0.08 to 0.12 (Table 3).

346 The change in soil moisture during El Niño is generally tracking that of precipitation
347 based on the ratio of ΔSM to ΔP . Both ΔSM to ΔP were normalized by their respective 1979



348 to 2016 mean value prior to calculating the ratio (Fig. 7a and Fig. 7b). Major exceptions to
349 precipitation tracking soil moisture occurred in the Cluster-4 region where the mean
350 direction of change in precipitation was opposite that of soil moisture during OND 1982 and
351 2015, as well as JFM 1998 (Table 4). Moreover, the mean magnitude of soil moisture change
352 was greater than 12 times that of precipitation, which was at least 2.5 times larger than the
353 magnitude difference reported for other regions. Much of these anomalies are attributed to
354 the lack of agreement between precipitation and soil moisture direction of change occurring
355 in the southern Amazon Basin, Latin America and equatorial Africa including the Sahel. An
356 amplified soil moisture response, particularly in the Sahel during OND 1997 and the
357 southern Amazon Basin during OND 1997 and 2015, may be an indication of an important
358 role of land-atmosphere interactions and/or temperature effects.

359 Similarly, the deviation of soil moisture is in general tracking that of
360 evapotranspiration based on the ratio of ΔSM to ΔET (Fig. 8a and Fig. 8b). Many of the same
361 exceptions to this pattern that were noted with precipitation were also observed here—the
362 mean direction of change in evapotranspiration was opposite to that of soil moisture
363 primarily in the Cluster-4 region during OND and JFM 1997-1998, as well as JFM 1983 (Table
364 5). The lack of agreement in the direction of evapotranspiration and soil moisture change is
365 also strongest in the southern Amazon Basin, Latin America and equatorial Africa including
366 the Sahel, particularly during OND 1997 and JFM 1998. Amplification of soil moisture
367 relative to evapotranspiration also occurred, especially in the southern Amazon Basin and
368 equatorial Africa during OND 1997 and JFM 1998.

369 The Pearson correlation coefficient (r) between GLDAS soil moisture and the Niño-
370 3.4 index for the humid tropics across the 38-year record is provided in Figure 9. In most



371 regions, there is an inverse relationship indicating the occurrence of El Niño leads to
372 decreased soil moisture within the tropics. The mean correlation over the clustered regions
373 are provided in Table 5, which indicates that the strongest mean negative correlations of -
374 0.12 and -0.09 occurred in Cluster-2 during OND and JFM, respectively. The Cluster-2 group
375 includes the Amazon Basin, Sahel, southeast Asia and maritime southeast Asia, many of
376 which were also shown to have the strongest and most consistent decreases in soil moisture
377 during the super El Niños. The strongest positive correlation of 0.05 occurred in Cluster-3
378 during JFM, which includes the southern Amazon Basin, east Africa and northern Australia.
379 These same regions also had the strongest and most consistent increases in soil moisture
380 during the super El Niños.

381 Figures 10a and 10b show the difference in OND and JFM soil moisture anomalies
382 with the addition of the bias correction that was developed using the in-situ data (e.g. Eq. 1
383 and Figure 1). For both OND and JFM, the application of the bias-corrected estimate
384 effectively led to a strengthening of the change in soil moisture anomalies relative to the
385 original GLDAS estimates. The strengthening of the magnitude generally falls between -0.05
386 and +0.05 with higher values occurring in regions where the original change in soil moisture
387 anomaly magnitude is higher in Figures 5a and 5b, such as the northeast Amazon Basin and
388 east Africa.

389

390 **Discussion**

391 Our findings generally agree with Miralles et al., (2014) who also reported a decrease
392 in soil moisture over the eastern Amazon Basin, Sahel, mainland southeast Asia and northern
393 Australia, as well as an increase over east Africa. Similar to van Schaik et al., (2018), we found



394 more acute reductions in soil moisture over the northeastern part of the Amazon Basin
395 during OND, but the center of these reductions shifted further west during JFM. This is shown
396 in Figures 5a and 5b as well as Cluster-2 in Figures 6a and 6b, which indicates the decrease
397 in soil moisture anomaly reached a maximum of 0.24 over the Cluster-2 region. However,
398 our methods allowed for a spatially continuous estimate across regions as well as an
399 assessment of soil moisture across seasons (e.g. OND vs. JFM), while focusing on super El
400 Niño events. As a result, we found several key differences in the soil moisture response to El
401 Niño relative to previous studies. Specifically, this includes increases in the soil moisture
402 anomaly of up to 0.20 over Latin America during OND, decreases in the soil moisture
403 anomaly of up to 0.24 over the Sahel during OND, decreases in the soil moisture anomaly of
404 up to 0.24 over maritime regions of southeast Asia during both OND and JFM, as well as
405 increases in the soil moisture anomaly of up to 0.20 over southern India during OND and
406 northern Australia during JFM.

407 The southern Amazon Basin stuck out as one region where the direction or magnitude
408 of change in soil moisture did not necessarily match that of precipitation or
409 evapotranspiration. This may in part be due to the distinction in climate impacts between
410 the northern and southern Amazon Basins during an El Niño event. The northern Amazon
411 Basin is influenced by displacement of the Intertropical Convergence Zone (ITCZ) and
412 changes in the Hadley cell positioning during this time, which forces the ITCZ northward
413 resulting in a reduction of rainfall (Marengo, 1992). However, the southern Amazon Basin is
414 primarily dependent on the South Atlantic Convergence Zone (SACZ), which is not as
415 influenced by El Niño. In general, during the peak El Niño season the intensification of the
416 SACZ enhances the southerly flow of low-level jets (LLJs). Circulation blockages produced by



417 the Andes help to channelize and intensify the LLJs over the southern Amazon Basin,
418 resulting in LLJs having primary control on temperature and precipitation regimes within
419 the region during the austral summer. Consequently, the southern Amazon Basin actually
420 experiences more rain during this time, but predictability of the timing and magnitude of this
421 sequence events and associated impacts on rainfall is generally lower than that of El Niño for
422 the northern Amazon (Marengo et al., 2002; Marengo et al., 2004). Moreover, rainfall
423 processes in the southern Amazon Basin depend on the displacement of cold fronts and
424 mesoscale circulation patterns, which occur at the synoptic scale. Thus, the lack of agreement
425 between precipitation and evapotranspiration change with soil moisture change in this
426 region occurs because of the strong impacts of atmospheric processes that originate outside
427 of this region (Silva Dias et al., 2002).

428 The spatial patterns we identified indicate that the relationship between soil
429 moisture and El Niño is more nuanced than what is revealed from the correlation of soil
430 moisture with the Niño-3.4 index. Although this analysis still indicates much of South
431 America, mainland southeast Asia and nearby islands respond most strongly to El Niño, the
432 pixels with stronger correlations do not precisely align with the regions identified where the
433 most consistent directional change during the three super El Niño events was observed. For
434 example, weak correlations ($|r| < 0.2$) between soil moisture and Niño-3.4 were identified
435 throughout the Sahel, Latin America and mainland southeast Asia during both OND and JFM,
436 despite portions of these regions showing a consistent positive or negative change in soil
437 moisture during super El Niño events. Several factors might be contributing to this issue.
438 First, as shown in Figures 1 and 2, the Sahel shows more widespread decreases in soil
439 moisture during OND, but increases during JFM. Thus, the inverse weak correlation in this



440 region might be occurring due to contrasting changes in soil moisture brought on by El Niño
441 during the first and second halves of the peak El Niño season. Second, we targeted the three
442 most recent super El Niños to evaluate the tropical soil moisture response, while the Niño-
443 3.4 index does not distinguish between the magnitude or type (e.g. CP or EP) of El Niño (Kao
444 and Yu, 2009; Yu and Zou, 2013). As such, the correlations shown in Figure 8 are more
445 representative of mean El Niño conditions, while the soil moisture changes depicted in
446 Figures 5a and 5b are representative of super El Niño conditions. We refrained from
447 conducting the correlation between soil moisture and the Niño-3.4 index using only months
448 when the three super El Niños occurred because this would severely limit the number of
449 observations available for use in the analysis. Another potential issue is related to the
450 accuracy of the GLDAS soil moisture response to El Niño for the tropics, which was dealt with
451 through comparison to in-situ observations.

452 Although the bias correction applied to GLDAS soil moisture shown in Figures 2 and
453 3 were able to substantially reduce the RMSE between in-situ observations and GLDAS
454 estimates, the overall performance of GLDAS in terms of r^2 is still mixed. Ten of the in-situ
455 sites that were evaluated had an $r^2 > 0.4$, while four had an $r^2 < 0.1$ (Figure 4). The large
456 disagreement between in-situ data and GLDAS for some locations is likely to be the result of
457 a mismatch in scale between these two datasets. As a result, GLDAS pixels with greater
458 topography, land cover or soil heterogeneity are less likely to match in-situ observations. For
459 instance, in the Manaus region of central Amazon, soils can vary from greater than 90% clay
460 on plateaus to greater than 90% sand in valleys at a horizontal distance of only 500 m and
461 the soil moisture can vary from over 100% in this span (Chauvel et al., 1987; Tomasella et
462 al., 2008; Cuartas et al., 2012). During dry periods such as those that typify a peak super El



463 Niño event for this region, strong variations in soil moisture have been detected at depths of
464 up to 5 m (Broedel et al., 2017). Because the maximum soil depth represented by GLDAS is
465 restricted to more shallow soil layers, the soil moisture variability represented in GLDAS for
466 this region should be taken with caution. Ideally, multiple in-situ observations at greater soil
467 depths could be used for comparison to each GLDAS pixel that was tested, but this level of
468 data coverage is generally not available for soil moisture, particularly in tropical regions
469 (Brocca et al., 2017). Although GLDAS also includes a 0.25-degree soil moisture product, the
470 higher spatial resolution data only includes estimates from one model and does not provide
471 estimates from all three of the most recent super El Niños.

472 Given the bias observed in the GLDAS soil moisture product relative to in-situ data
473 over the available record, we also compared soil moisture estimates from GLDAS to in-situ
474 data only during the mature phase 2015-16 super El Niño event to confirm that a similar bias
475 occurred during this period. The variability of in-situ estimates captured by GLDAS differed
476 by no more than 2% when considering only the peak El Niño months of the 2015-16 event,
477 thereby demonstrating that the variability in bias between the two periods was minimal.
478 Given the higher number of observations when all months were used (e.g. $n = 802$ versus only
479 $n = 67$), we chose to base the bias-corrected estimate on the comparison made using all
480 available months of data to incorporate a greater number of observations into the analysis.

481 Several strategies exist that can increase confidence in soil moisture estimates from
482 data products like GLDAS. First, in-situ observations of soil moisture need to improve in both
483 space and time to evaluate and constrain the land surface models used in GLDAS. The
484 distribution of soil moisture observations is much lower in tropical regions than other areas
485 (Brocca et al., 2017), which is not surprising given the dearth of hydrologic observations



486 available from developing countries in tropical regions (Alsdorf et al., 2007) coupled with
487 the reported decrease in hydrologic monitoring across sites worldwide (McCabe et al.,
488 2017). In addition, increased participation in contributing in-situ soil moisture data to online
489 databases such as FLUXNET (ORNL DAAC, 2017b) and ISMN (Dorigo et al., 2011; Dorigo et
490 al., 2013) would help alleviate the limited access to observational datasets.

491 Satellite observations of soil moisture can also be used to fill this gap, but a number
492 of issues exist with historical satellite derived estimates of soil moisture. Substantial biases
493 exist in retrieval algorithms (Entekhabi et al., 2010) and direct estimates are restricted to
494 shallow soil depths are of limited value when soil moisture at greater depths is needed
495 (McCabe et al., 2017). Such shortcomings have encouraged investigations into the relative
496 influence of vegetation, soil and topography on soil moisture dynamics to better upscale
497 point-based measurements of soil moisture to larger, remotely sensed scales (Gaur and
498 Mahanty, 2016). Algorithms have been developed to interpolate shallow subsurface
499 estimates of soil moisture to the root zone, but a recent global evaluation of the accuracy of
500 the algorithms being used for this purpose to generate Soil Moisture Active Passive (SMAP)
501 Level 4 data was limited to 17 sites with only one occurring within the tropical climate zone
502 (Reichle et al., 2017). Moreover, satellite radar used to observe soil moisture from many
503 historical missions fails to penetrate dense rainforest canopies making this data of limited
504 use for many tropical regions. Another issue with satellites is the limited lifetime of the
505 mission coupled with the lack of follow-on missions that would enable extension of the
506 observation record so impacts from cyclical climate events like ENSO that occur on decadal
507 timescales can be adequately assessed. As a result, data is often combined from multiple
508 missions to extend satellite records, which can introduce additional error (Gruber et al.,



509 2019). Access to more spatially and temporally continuous global soil moisture data from
510 satellites or assimilation products are thus paramount to improve the spatial and temporal
511 resolution of soil moisture estimates and enable better prediction of soil moisture behavior
512 over long timescales (Brocca et al., 2017).

513 Lastly, the current GLDAS product is produced mainly by running offline land surface
514 models forced with atmospheric data from a combination of rain gauge, satellite, and radar
515 precipitation estimates and outputs (e.g., radiation) from numerical prediction models.
516 Uncertainties and biases in the land models and forcing data can contribute importantly to
517 uncertainties and biases in the GLDAS soil moisture (Piao et al., 2013). Future products that
518 assimilate in-situ and remotely-sensed observations of terrestrial energy and water storages
519 such as soil moisture and snow and fluxes such as evapotranspiration, sensible heat flux, and
520 runoff will likely further improve the quality of GLDAS soil moisture for better
521 characterization of impacts from El Niño (e.g. Albergel et al., 2012; Gruber et al., 2018). This
522 has important implications for understanding water resources and plant response to ENSO
523 events, given the role of soil moisture in climate extremes due to feedbacks with the
524 atmosphere (Seneviratne et al., 2010).

525

526 **Summary and Conclusion**

527 We describe the response of soil moisture in the humid tropics to El Niño while
528 focusing on impacts from the three most recent super El Niños of 1982-83, 1997-98 and
529 2015-16 using soil moisture estimates from GLDAS. The largest and most consistent
530 reductions in the soil moisture anomaly of up to 0.24 occurred over the northern Amazon
531 basin and the maritime regions of southeast Asia, Indonesia and New Guinea. The soil



532 moisture response is largely consistent with the precipitation and evapotranspiration
533 responses, as indicated by the overwhelmingly positive ratio of soil moisture change to both
534 precipitation and evapotranspiration change over the same period in regions with consistent
535 soil moisture response. Some notable exceptions include the Sahel and southern Amazon
536 Basin where a greater number of pixels show the direction of change for soil moisture is
537 opposite that of precipitation and evapotranspiration. The soil moisture change was
538 amplified relative to precipitation and evapotranspiration in these areas particularly during
539 OND, suggesting that the soil moisture response may be amplified through land-atmosphere
540 interactions and/or the temperature response and differing climate patterns between the
541 north and south Amazon Basin. Indeed, land-atmosphere interactions have been suggested
542 to play more of an important role in the regional water cycle over the Amazon and Sahel (e.g.,
543 Koster et al. 2004; Wang et al., 2013; Levine et al., 2019), so their role in the soil moisture
544 response to El Niño deserves more investigation over these regions in the future.

545 Comparison of GLDAS estimates to in-situ data from 16 reference sites to gauge the
546 utility of these estimates in large scale models reveals a high degree of variability in the
547 performance of GLDAS among the different sites. Although some of the poor performance
548 can invariably be explained by a mismatch in the scale of in-situ observations to the coarse,
549 1-degree resolution of GLDAS, improvements in the availability of ground-based soil
550 moisture observations and access to more data from temporally-continuous, global soil
551 moisture observing satellite missions that allow for estimates beneath dense rain forest
552 canopies are necessary to improve upon these estimates by constraining land model
553 estimates through data assimilation. Such an effort will be useful to increase the accuracy of



554 tropics hydrology and ecosystem models to make better predictions of El Niño impacts on
555 land surface hydrology.

556

557 **Acknowledgements**

558 This project was supported as part of the Next Generation Ecosystem Experiments-
559 Tropics, funded by the United States Department of Energy, Office of Science, Office of
560 Biological and Environmental Research through the Terrestrial Ecosystem Science Program.
561 Data obtained from French Guiana were recorded thanks to an “investissement d’avenir”
562 grant from the Agence Nationale de la Recherche (CEBA, ref ANR-10-LABX-25-01; ARBRE,
563 ref. ANR-11-LABX-0002-01). Data obtained from one of the Panama sites were recorded
564 thanks to an award from the National Science Foundation (NSF 1360305). Global soil
565 moisture data products used in this study are publicly available at the following locations:

- 566 • GLDAS: <https://disc.gsfc.nasa.gov/datasets?page=1&keywords=GLDAS>
- 567 • ERA5: <https://cds.climate.copernicus.eu/#!/home>
- 568 • MERRA2: https://gmao.gsfc.nasa.gov/reanalysis/MERRA-2/data_access/
- 569 • GLEAM: <https://www.gleam.eu/#downloads>

570 In-situ data collected from Indonesia was made possible by the Deutsche
571 Forschungsgemeinschaft (DFG, German Research Foundation) – project number 192626868
572 – SFB 990 and the Ministry of Research, Technology and Higher Education (Ristekdikti) in
573 the framework of the collaborative German – Indonesian research project CRC990. We
574 would also like to thank Charu Varadharajan for providing valuable assistance with database
575 access and guidance on data storage during the course of this research. The Pacific Northwest



576 National Laboratory is operated for the Department of Energy by Battelle Memorial Institute under
577 contract DE-AC05-76RL01830.

578

579

580 **References**

581

582 Acker, J. G. and Leptoukh, G., "Online analysis enhances use of NASA earth science data", EOS, Trans. AGU, 88, p.
583 14 and 17, 2007.

584

585 Albergel, C., and Coauthors, Evaluation of remotely sensed and modelled soil moisture products using global
586 ground-based in situ observations, Rem. Sens. Environ., 118, 215-226, 2012.

587

588 Ashok, K., Behera, S. K., Rao, S. A., Weng, H., and Yamagata, T., El Niño Modoki and its possible teleconnection, J.
589 Geophys. Res., 112, 1-27, 2007.

590

591 Banholzer, S. and Donner, S., The influence of different El Niño types on global average temperature, Geophys.
592 Res. Lett., 41, 2093-2099, 2014.

593

594 Beringer, J., Hutley, L. B., Tapper, N. J., and Cernusak, L. A., Savanna fires and their impact on net ecosystem
595 productivity in North Australia, Glob Change Biol., 13, 990-1004, 2007.

596

597 Beringer, J., and Coauthors, Special—Savanna patterns of energy and carbon integrated across the landscape,
598 Bull. Amer. Meteorol. Soc., 92, 1467-1485, 2011.

599

600 Beringer, J., Livesley, S. J., Randle, J., Hutley, L. B., Carbon dioxide fluxes dominate the greenhouse gas exchanges
601 of a seasonal wetland in the wet-dry tropics of northern Australia, Ag. For. Meteorol., 182-183, 239-
602 247, 2013.

603

604 Bonal, D., and Coauthors, Impact of severe dry season on net ecosystem exchange in the Neotropical rainforest
605 of French Guiana, Glob. Chang. Biol., 14, 1917-1933, 2008.

606

607 Bretfeld, M., Ewers, B. E., and Hall, J. S., Plant water use responses along secondary forest succession during the
608 2015–2016 El Niño drought in Panama. New Phytol. 219, 885-899, 2018.

609

610 Brocca, L., Ciabatta, L., Massari, C., Camici, S., and Tarpanelli, A., Soil moisture for hydrological applications:
611 open questions and new opportunities, Water, 9, 140, 1-20, 2017.

612

613 Broedel, E., Tomasella, J., Cândido, L. A., and Randow, C. V., Deep soil water dynamics in an undisturbed primary
614 forest in central Amazonia: differences between normal years and the 2005 drought, Hydrol. Process.,
615 31, 1749-1759, 2017.

616

617 Bunge, L. and Clarke, A. J., A verified estimation of the El Niño Index Niño-3.4 since 1877, J. Clim., 22, 3979-3992,
618 2009.

619

620 Caliński, T. and Harabasz, J., A dendrite method for cluster analysis, Comm. Stat. Theor. M., 3, 1-27, 1972.

621

622 Charrad, M., Ghazzali, N., Boiteau, V., and Niknafs, A., NbClust: An R package for determining the relevant
623 number of clusters in a data set, J. Stat Softw, 61, 1-36, 2014.

624



- 625 Chauvel, A., Lucas Y., and Boulet, R., On the genesis of the soil mantle of the region of Manaus, Central Amazonia,
626 Brazil, *Experientia*, 43, 234-241, 1987.
- 627
- 628 Chen, L., Li, T., Wang, B., and Wang, L., Formation mechanism for 2015/16 super El Niño, *Sci. Rep.*, 7, 1-10, 2017.
629
- 630 Chou, C., Huang, L. -F., Tu, J. -Y., Tseng, L., and Hsueh, Y. -C., El Niño impacts on precipitation in the western
631 North Pacific-East Asian Sector, *J. Clim.*, 22, 2039-2057, 2009.
- 632
- 633 Copernicus Climate Change Service (C3S), ERA5: Fifth generation of ECMWF atmospheric reanalyses of the
634 global climate, Copernicus Climate Change Service Climate Data Store (CDS), 10 April 2019,
635 <https://cds.climate.copernicus.eu/cdsapp#!/home>, 2017.
- 636
- 637 Cuartas, L. A., and Coauthors, Distributed hydrological modeling of a micro-scale rainforest watershed in
638 Amazonia: model evaluation and advances in calibration using the new HAND terrain model, *J.*
639 *Hydrol.*, 462-463, 15-27, 2012.
- 640
- 641 Dai, A. and Wigley, T. M. L., Global patterns of ENSO-induced precipitation, *Geophys., Res. Lett.*, 27, 1283-
642 1286, 2000.
- 643
- 644 Dai, Y., and Coauthors, The common land model (CLM), *Bull. Am. Meteorol. Soc.*, 1013-1024, 2003.
- 645
- 646 Davies, D. L., and Bouldin, D. W., A cluster separation measure, *IEEE Trans. Pattern Anal. Mach. Intell.*, 1, 224-
647 227, 1979.
- 648
- 649 Dorigo, W. A., and Coauthors, The International Soil Moisture Network: a data hosting facility for global in situ
650 soil moisture measurements, *Hydrol. Earth Syst. Sci.*, 15, 1675-1698, 2011.
- 651
- 652 Dorigo, W. A., and Coauthors, Global automated quality control of in-situ soil moisture data from the
653 International Soil Moisture Network, *Vadose Zone J.*, 12, 2013.
- 654
- 655 Dorigo, W. A., and Coauthors, ESA CCI Soil Moisture for improved Earth system understanding: State-of-the-art
656 and future directions, *Rem. Sens. Environ.*, 203, 185-215, 2017.
- 657
- 658 Dunn, J., Well separated clusters and optimal fuzzy partitions, *J. Cybern.*, 4, 95-104, 1974.
- 659
- 660 Ek, M., and Coauthors, Implementation of Noah land surface model advances in the National Centers for
661 Environmental Prediction operational mesoscale Eta model, *J. Geophys. Res.*, 108, 1-16, 2003.
- 662
- 663 Entekhabi, D., Reichle, R. H., Koster, R. D., and Crow, W. T., Performance metrics for soil moisture retrievals and
664 application requirements, *J. Hydrometeor.*, 11, 832-840, 2010.
- 665
- 666 Gaur, N., and Mohanty, B. P., Land-surface controls on near-surface soil moisture dynamics: traversing remote
667 sensing footprints, *Water Resour. Res.*, 52, 6365-6385, 2016.
- 668
- 669 Gelaro, R., and Coauthors, The Modern-Era Retrospective Analysis for Research and Applications, Version 2
670 (MERRA-2), *J. Clim.*, 30, 5419-5454, 2017.
- 671
- 672 Goulden, M. L., and Coauthors, Diel and seasonal patterns of tropical forest CO₂ exchange, *Ecol. Appl.*, 14, S42-
673 S54, 2004.
- 674
- 675 Green, J. K., Seneviratne, S. I., Berg, A. M., Findell, K. L., Hagemann, S., Lawrence, D. M., and Gentine, P., Large
676 influence of soil moisture on long-term terrestrial carbon uptake, *Nature*, 565, 476-479, 2019.
- 677
- 678 Gruber, A., Crow W. T., and Dorigo, W. A., Assimilation of spatially sparse in situ soil moisture networks into a
679 continuous model domain, *Water Resour. Res.*, 54, 1353-1367, 2018.
- 680



- 681 Gruber, A., Scanlon, T., van der Schalle, R., Wagner, W., and Dorigo, W. A., Evolution of the ESA CCI Soil Moisture
682 climate data records and their underlying merging methodology, *Earth Syst. Sci. Data*, 11, 717-739,
683 2019.
684
- 685 Halkidi, M., Vazirgiannis, M., and Batistakis, I., Quality scheme assessment in the clustering process, In: Zighed
686 D.A., J. Komorowski and J. Żytkow (eds), *Principles of data mining and knowledge discovery, PKDD*
687 2000, Lecture notes in computer science, vol 1910, Springer, Berlin, Heidelberg, 2000.
688
- 689 Halkidi M, Vazirgiannis, M., Clustering validity assessment: finding the optimal partitioning of a data set,
690 *Proceedings of the 2001 IEEE International Conference on Data Mining*, 187-194, 2001.
691
- 692 Hameed, S. N., Jin, D., and Thilakan, V., A model for super El Niños, *Nat. Comm.*, 9, 1-15, 2018.
693
- 694 Hong, L. -C., LinHo, and Jin, F. -F., A Southern Hemisphere booster of super El Niño, *Geophys. Res. Lett.*, 41, 2142-
695 2149, 2014.
696
- 697 Huang, B., L'Heureux, M., Hu, Z. -Z., and Zhang, H. -M., Ranking the strongest ENSO events while incorporating
698 SST uncertainty, *Geophys. Res. Lett.*, 43, 9165-9172, 2016.
699
- 700 Huang, P. and Chen, D., Enlarged asymmetry of tropical Pacific rainfall anomalies induced by El Niño and La
701 Niña under global warming, *J. Clim.*, 30, 1327-1343, 2017.
702
- 703 Hubert, L. J., and Levin, J. R., A general statistical framework for assessing categorical clustering in free recall,
704 *Psychol. Bull.*, 83, 1072-1080, 1976.
705
- 706 Iizumi, T., and Coauthors, Impacts of El Niño Southern Oscillation on the global yields of major crops, *Nat.*
707 *Comm.*, 5, 1-7, 2014.
708
- 709 Jiménez-Muñoz, J. C., Mattar, C., Barichivich, J., Santamaria-Artigas, A., Takahashi, K., Malhi, Y., Sobrino, J. A., and
710 van der Schrier, G., Record-breaking warming and extreme drought in the Amazon rainforest during
711 the course of El Niño 2015-16, *Sci. Rep.*, 6, 1-7, 2016.
712
- 713 Jardine, K., and Coauthors, Raw/translated data and metadata from sensor measurements at Manaus, Brazil,
714 15 Feb 2015 - 14 July 2016, *NGEE Tropics Data Collection*, Accessed at
715 <http://dx.doi.org/10.15486/ngt/1507764>, 2019.
716
- 717 Jones, P. D., Osborn, T. J. and Briffa, K. R., The evolution of climate over the last millennium, *Science*, 292, 662-
718 667, 2001.
719
- 720 Kang, C. S., Kanniah, K. D., Kerr, Y. H., and Cracknell, A. P., Analysis of in-situ soil moisture data and validation of
721 SMOS soil moisture products at selected agricultural sites over a tropical region, *Int'l J. Rem. Sens.*, 37,
722 3636-3654, 2016.
723
- 724 Kao, H. -Y. and Yu, J. -Y., Contrasting Eastern-Pacific and Central-Pacific Types of ENSO, *J. Clim.*, 22, 615-632,
725 2009.
726
- 727 Köhli, M., Schrön, M., Zreda, M., Schmidt, U., Dietrich, P., and Zacharias, S., Footprint characteristics revised for
728 field-scale soil moisture monitoring with cosmic-ray neutrons, *Water Resour. Res.*, 51, 5772-5790,
729 2017.
730
- 731 Koster, R. D., and Coauthors, Regions of strong coupling between soil moisture and precipitation. *Science*, 305,
732 1138-1140, 2004.
733
- 734 Koster, R., and Suarez, M., Energy and water balance calculations in the Mosaic LSM NASA Tech Memo, 104606,
735 p. 76, 1996.
736



- 737 Kottek, M., Grieser, J., Beck, C., Rudolf, B., and Rubel, F., World Map of the Köppen-Geiger climate classification
738 updated, *Meteorol. Z.*, 15, 259-263, 2006.
739
- 740 Kranowski, W. J. and Lai, Y. T., A criterion for determining the number of groups in a data set using sum-of-
741 squares clustering, *Biometrics*, 44, 23-34, 1998.
742
- 743 Kug, J. -S., Jin, F. -F., and An, S. -I., Two types of El Niño events: cold tongue El Niño and warm pool El Niño, *J.*
744 *Clim.*, 22, 1499-1515, 2009.
745
- 746 Larkin, N. K. and Harrison, D. E., Global seasonal temperature and precipitation anomalies during El Niño
747 autumn and winter, *Geophys. Res. Lett.*, 32, 1-4, 2005.
748
- 749 Larson, K. M., Small, E. E., Gutmann, E. D., Bilich, A. L., Braun, J. J., and Zavorotny, V. U., Use of GPS receivers as a
750 soil moisture network for water cycle studies, *Geophys. Res. Lett.*, 35, 1-5, 2008.
751
- 752 Levine, P. A., Randerson, J. T., Chen, Y., Pritchard, M. S., Xu, M. and Hoffman, F. M., Soil moisture variability
753 intensifies and prolongs eastern Amazon temperature and carbon cycle response to El Niño-Southern
754 Oscillation, *J. Clim.*, 32, 1273-1292, 2019.
755
- 756 L'Heureux, M. L., Tippet, M. K. and Barnston, A. G., Characterizing ENSO coupled variability and its impact on
757 North American seasonal precipitation and temperature, *J. Clim.*, 28, 4231-4245, 2015.
758
- 759 Liang, X., Lettenmaier, D. P., Wood, E. F., and Burges, S. J., A simple hydrologically based model of land surface
760 water and energy fluxes for general circulation models, *J. Geophys. Res.*, 99, 14415-14428, 1994.
761
- 762 Liu, Y. Y., Dorigo, W. A., Parinussa, R. M., de Jeu, R.A.M., Wagner, W., McCabe, M.F., Evans, J.P., and van Dijk,
763 A.I.J.M., Trend-preserving blending of passive and active microwave soil moisture retrievals, *Rem.*
764 *Sens. Environ.*, 123, 280-297, 2012.
765
- 766 Marengo, J., Interannual variability of surface climate in the Amazon basin, *Int. J. Clim.*, 12, 853-863, 1992.
767
- 768 Marengo, J. A., Douglas, M. W., and Silva Dias, P. L., The South American low-level jet east of the Andes during
769 the 1999 LBA-TRMM and LBA-WET AMC campaign, *J. Geophys. Res.*, 107, 1-11, 2002.
770
- 771 Marengo, J. A., Soares, W. R., Saulo, C., and Nicolini, M., Climatology of the low-level jet east of the Andes as
772 derived from the NCEP-NCAR Reanalyses: characteristics and temporal variability, *J. Clim.*, 17, 2261-
773 2280, 2004.
774
- 775 Martens, B., D. G., and Coauthors, GLEAM v3: satellite-based land evaporation and root-zone soil moisture,
776 *Geoscientific Model Development*, 10, 1903-1925, 2017.
777
- 778 McCabe, M. F. and Coauthors, The future of Earth observation in hydrology, *Hydrol. Earth Syst. Sci.*, 21, 2879-
779 3914, 2017.
780
- 781 McClain, J. O. and Rao, V. R., CLUSTISZ: A program to test for the quality of clustering of a set of objects, *J. Mark.*
782 *Res.*, 12, 456-460, 1975.
783
- 784 Meijide, A., Badu, C.S., Moyano, F., Tiralla, N., Gunawan, D., and Knohl, A., Impact of forest conversion to oil palm
785 and rubber plantations on microclimate and the role of the 2015 ENSO event, *Ag. For. Meteorol.*, 252,
786 208-219, 2018.
787
- 788 Milligan, G. W., An examination of the effect of six types of error perturbation on fifteen clustering algorithms,
789 *Psychometrika*, 45, 325-342, 1980.
790
- 791 Milligan, G., A Monte Carlo study of thirty internal criterion measures for cluster analysis, *Psychometrika*, 46,
792 187-199, 1981.



- 793
794 Miralles, D. G., and Coauthors, El Niño-La Niña cycle and recent trends in continental evaporation, *Nat. Clim.*
795 *Change*, 4, 122-126, 2014.
796
797 Miralles, D. G., and Coauthors, Global land-surface evaporation estimated from satellite-based observations,
798 *Hydrol. Earth Syst. Sci.*, 15, 453-469, 2011.
799
800 Ochoa-Sánchez, A., Crespo, P., and Célleri, R., Quantification of rainfall interception in the high Andean Tussock
801 grasslands, *Ecohydrol.*, 11, 2018.
802
803 ORNL DAAC, Spatial Data Access Tool (SDAT), ORNL DAAC, Oak Ridge, Tennessee, USA, Accessed 1 February,
804 2018, 2017a.
805
806 ORNL DAAC, Fluxnet: Archived Website Including Site and Investigator Information. ORNL DAAC, Oak Ridge,
807 Tennessee, USA, Accessed 1 February, 2018, 2017b.
808
809 Piao, S., and Coauthors, Evaluation of terrestrial carbon cycle models for their response to climate variability
810 and to CO₂ trends, *Glob. Change Biol.*, 19, 2117-2132, 2013.
811
812 Prigent, C., Aires, F., Rossow W. B., and Robock, A., Sensitivity of satellite microwave and infrared observations
813 to soil moisture at a global scale: relationship of satellite observations to in situ soil moisture
814 measurements, *Clim. Dyn.*, 110, 1-15, 2005.
815
816 Raddatz, T. J., and Coauthors, Will the tropical land biosphere dominate the climate-carbon cycle feedback
817 during the twenty-first century? *Clim. Dyn.*, 29, 565-574, 2007.
818
819 Ratkowsky, D. A. and Lance, G. A., A criterion for determining the number of groups in a classification, *Aust.*
820 *Comput. J.*, 10, 115-117, 1978.
821
822 Reichle, R. H., and Coauthors, Assessment of the SMAP Level-4 surface and root-zone soil moisture product
823 using in situ measurements, *J. Hydrometeorol.*, 18, 2621-2645, 2017.
824
825 Rodell, M., and Coauthors, The global land data assimilation system, *Bull. Amer. Meteor. Soc.*, 85, 381-394, 2004.
826
827 Ropelewski, C. F., and Halpert, M. S., Precipitation patterns associated with the high index phase of the Southern
828 Oscillation, *J. Clim.*, 2, 268-284, 1989.
829
830 Rousseeuw, P. J., Silhouettes: a graphical aid to the interpretation and validation of cluster analysis, *J. Comput.*
831 *Appl. Math.*, 20, 53-65, 1987.
832
833 Rubio, V. E. and Detto, M., Spatiotemporal variability of soil respiration in a seasonal tropical forest, *Ecol. Evol.*,
834 7104-7116, 2017.
835
836 Sarle, W. S., The cubic clustering criterion, In SAS technical report A-108, Cary, NC: SAS Institute, 1983.
837
838 Silva Dias, M. A. F., and Coauthors, Clouds and rain processes in a biosphere-atmosphere interaction context in
839 the Amazon Region, *J. Geophys. Res.*, 107, 8072, 1-17, 2002.
840
841 van Schaik, E., Killars, L., Smith, N. E., Koren, G., van Beek, L. P. H., Peters, W., and van der Laan-Luijkx, I.T.,
842 Changes in surface hydrology, soil moisture, and gross primary production in the Amazon during the
843 2015/2016 El Niño. *Phil. Trans. R. Soc. B* 373, 1-9, 2018.
844
845 Schaefer, G. L., Cosh, M. H., and Jackson, T.J., The USDA Natural Resources Conservation Service Soil Climate
846 Analysis Network (SCAN), *J. Atmos. Ocean. Tech.*, 24, 2073-2077, 2007.
847



- 848 Schubert, S. D., and Coauthors, Global meteorological drought: a synthesis of current understanding with a focus
849 on SST drivers of precipitation deficits, *J. Clim.*, 29, 3989-4019, 2016.
850
851 Seneviratne, S. I., and Coauthors, Investigating soil moisture-climate interactions in a changing climate: A
852 review, *Earth Sci. Rev.*, 99, 125-161, 2010.
853
854 Takahashi, K., Montecinos, A., Goubanova K., and Dewitte, B., ENSO regimes: reinterpreting the canonical and
855 Modoki El Niño, *Geophys. Res. Lett.*, 38, 1-5, 2011.
856
857 Tebaldi, C. and Knutti, R., The use of multi-model ensemble in probabilistic climate projections, *Philos. Trans.
858 R. Soc.*, 365, 2053-2075, 2007.
859
860 Tomasella, J., and Coauthors, The water balance of an Amazonian micro-catchment: the effect of interannual
861 variability of rainfall on hydrological behavior, *Hydrol. Process.*, 22, 2133-2147, 2008.
862
863 Trenberth, K. E., The definition of El Niño, *Bull. Amer. Meteor. Soc.*, 78, 2771-2778, 1997.
864
865 Wanders, N., and Coauthors, Forecasting the hydroclimatic signature of the 2015/16 El Niño event on the
866 western United states, *J. Hydrometeor.*, 18, 177-186, 2017.
867
868 Wang, W., and Coauthors, Variations in atmospheric CO₂ growth rates coupled with tropical temperature, *Proc.
869 Nat. Acad. Sci.*, 110, 13061-13066, 2013.
870
871 Wang, C., Deser, C., Yu, J. -Y., DiNezio, P., and Clement, A., El Niño and Southern Oscillation (ENSO): A review.
872 Coral Reefs of the Eastern Tropical Pacific: Persistence and Loss in a Dynamic Environment, Glynn, P.
873 W., Manzello, D. P., and Enoch, I. C., Eds., *Coral Reefs of the World*, Vol. 8, Springer, 85-106, 2017.
874
875 Wu, J., and Coauthors, Leaf development and demography explain photosynthetic seasonality in Amazon
876 evergreen forests, *Science*, 351, 972-976, 2016.
877
878 Xu, K., Tam, C.-Y., Zhu, C., Liu, B., and Wang, W., CMIP5 projections of two types of El Niño and their related
879 tropical precipitation in the twenty-first century, *J. Clim.*, 30, 849-864, 2017.
880
881 Yu, J. -Y. and Kim, S. T., Short communication identifying the types of major El Niño events since 1870, *Int. J.
882 Climatol.*, 33, 2105-2112, 2013.
883
884 Yu, J. -Y. and Zou, Y., The enhance drying effect of Central-Pacific El Niño on US winter, *Environ. Res. Lett.*, 8, 1-
885 7, 2013.
886
887 Zhuo, L., Dai, Q., Islam T., and Han, D., Error distribution modelling of satellite soil moisture measurements for
888 hydrological applications, *Hydrol. Proc.*, 30, 2223-2236, 2016.
889

893 **Tables**

894 **Table 1:** Information on geospatial location, record length and monitoring instruments used
895 for in-situ observations that were used in the analysis.

896



897 **Table 2:** Mean ranking of proposed cluster groups across OND and JFM during three super
898 El Niños for tests used in R package NbClust (version 3.0). Low scores denote highest
899 ranking.

900

901 **Table 3:** Mean and standard deviation of October to December (OND) and January to March
902 (JFM) change in the GLDAS soil moisture for clustered regions in the humid tropics. Statistics
903 computed using OND and JFM GLDAS soil moisture anomalies during El Niño years 1982-83,
904 1997-98, and 2015-16 relative to the 1979-2016 mean.

905

906 **Table 4:** Mean and standard deviation of October to December (OND) and January to
907 March (JFM) change in soil moisture to precipitation ratio for the same regions shown
908 in Table 3. Statistics computed using OND and JFM GLDAS soil moisture anomalies
909 during El Niño years 1982-83, 1997-98, and 2015-16 relative to the 1979-2016 mean.

910

911 **Table 5:** Mean and standard deviation of October to December (OND) and January to March
912 (JFM) change in soil moisture to evapotranspiration ratio for the same regions shown in
913 Table 3. Statistics computed using OND and JFM GLDAS soil moisture anomalies during El
914 Niño years 1982-83, 1997-98, and 2015-16 relative to the 1979-2016 mean.

915

916 **Table 6:** Mean and standard deviation of 1979-2016 GLDAS soil moisture correlation with
917 the Niño3.4 index for the same regions shown in Table 3.

918

919



920 **Figures**

921 **Figure 1:** 1979-2017 monthly time series of mean soil moisture across all in-situ data
922 locations shown in Table 1 for multiple data products including the GLDAS multi-model
923 mean (black, solid), MERRA2 (red, solid), ERA5 (blue, solid), and GLEAM (green, solid), as
924 well as the individual land surface models that make up GLDAS NOAH (black, short dash),
925 MOSAIC (black, dot), VIC (black, dash dot) and CLM (black, long dash). Note that the GLEAM
926 time series starts from 1980.

927

928 **Figure 2:** In-situ soil moisture vs. GLDAS soil moisture during October to December (OND)
929 and January to March (JFM) for El Niño years 1982-83, 1997-98, and 2015-16. Each circle
930 corresponds to one in-situ data point in space and time. The left panel includes data from all
931 18 sites shown in Table 1, with data from Australia, Ecuador, and Brazil highlighted in blue,
932 red, and green, respectively. The right panel shows the same information with the Ecuador,
933 Australia, and Brazil site data removed. The blue dashed line and red solid line represent
934 the 1:1 line and the regression line, respectively.

935

936 **Figure 3:** Bias-corrected soil moisture estimates from GLDAS relative to in-situ soil
937 moisture observations for all sites with the mean RMSE shown in red.

938

939 **Figure 4:** Bias-corrected estimate from GLDAS (black line) and in-situ observation (red line)
940 of soil water content for 16 individual locations in the humid tropics. RMSE and r^2 coefficient
941 of determination for each location are also shown.

942



943 **Figure 5a:** October to December (OND) change in GLDAS soil moisture anomalies during the
944 super El Niño years 1982 (top), 1997 (middle), and 2015 (bottom) relative to the previous
945 years. Anomalies relative to 1979-2016 period.

946

947 **Figure 5b:** Same as Figure 4a, but for January to March (JFM) in 1983 (top), 1998 (middle)
948 and 2016 (bottom).

949

950 **Figure 6a:** K-means cluster analysis results for October to December (OND) for 1982 (top),
951 1997 (middle) and 2015 (bottom). Corresponding histograms of soil moisture anomalies for
952 each of the four clusters also shown. Anomalies relative to 1979-2016 period.

953

954 **Figure 6b:** Same as Figure 5a, but for January to March (JFM) in 1983 (top), 1998 (middle)
955 and 2016 (bottom).

956

957 **Figure 7a:** Ratio of GLDAS soil moisture to precipitation change computed using October to
958 December (OND) anomalies during El Niño years 1982-83, 1997-98, and 2015-16 relative to
959 previous years. Anomalies relative to 1979-2016 period.

960

961 **Figure 7b:** Same as Figure 6a but for January to March in 1983 (top), 1998 (middle) and
962 2016 (bottom).

963



964 **Figure 8a:** Ratio of GLDAS soil moisture to evapotranspiration change computed using
965 October to December (OND) anomalies during El Niño years 1982-83, 1997-98, and 2015-
966 16 relative to previous years. Anomalies relative to 1979-2016 period.

967

968 **Figure 8b:** Same as Figure 7a but for January to March in 1983 (top), 1998 (middle) and
969 2016 (bottom).

970

971 **Figure 9:** Pearson correlation coefficient between GLDAS soil moisture and NINO3.4 index
972 from 1979 to 2016. Colors indicate regions where the mean correlation was negative (red)
973 and positive (blue).

974

975 **Figure 10a:** Difference in October to December (OND) change in GLDAS soil moisture
976 anomalies when bias correction is applied relative to no bias correction. Red pixels indicate
977 regions that showed a negative correlation increase, while blue regions indicate regions that
978 showed a positive correlation increase with the addition of the bias correction. Plots shown
979 for the super El Niño years 1982 (top), 1997 (middle), and 2015 (bottom).

980

981 **Figure 10b:** Same as Figure 9a but for January to March (JFM) in 1983 (top), 1998 (middle)
982 and 2016 (bottom).



Table 1: Information on geospatial location, record length and monitoring instruments used for in-situ observations that were used in the analysis.

Country	Lat (°N)	Long (°E)	Land Cover Type	Record Length (no. months) ¹	Elev (m)	Depth (cm)	Instrument ²
Australia (1)	-17.12	145.63	Rainforest	May 2014 – Mar 2017 (35)	715	28	COSMOS ⁴
Australia (2)	-14.16	131.39	Tropical Savanna	Jun 2011 – Dec 2016 (67)	7.5	38	COSMOS ⁴
Australia (3)	-13.08	131.12	Woody Savanna	Nov 2007 – May 2009 (19)	76	0-10	ECFT ⁵
Australia (4)	-12.49	131.15	Woody Savanna	Aug 2001 – Dec 2014 (161)	39	0-10	ECFT ⁶
Australia (5)	-12.55	131.31	Wetlands	Feb 2006 – Oct 2008 (33)	4	0-10	ECFT ⁷
Brazil ³ (1/2)	-2.61	-60.21	Evergreen Broadleaf Forest	Sep 2015 – Mar 2016 (14)	130	0-10	TDR ⁸
Brazil (3)	-3.02	-54.97	Evergreen Broadleaf Forest	Jul 2000 – Feb 2004 (44)	48	0-10	ECFT ⁹
Brazil (4)	-2.85	-54.97	Evergreen Broadleaf Forest	Dec 2008 – Apr 2016 (47)	200	50	TDR ¹⁰
Dom. Republic (1)	19.76	-70.57	Savanna	Feb 2013 – Aug 2017 (53)	-32	0-10	GPS ¹¹
Dom. Republic (2)	17.90	-71.67	Savanna	Feb 2013 – Dec 2016 (56)	-17	0-10	GPS ¹¹
Ecuador	-3.06	-79.24	Wet Páramo	Jan 2011 – Dec 2016 (72)	3,780	0-10	TDR ¹²
French Guiana ³	5.28	-52.92	Evergreen Broadleaf Forest	Jan 2007 – Jan 2017 (133)	20	0-10	ECFT ¹³
Indonesia	-1.97	102.60	Grassland	Jun 2013 – Sep 2017 (45)	48	30	TDR ¹⁴
Kenya	0.28	36.87	Savanna/Grassland	Oct 2011 – May 2017 (68)	1,824	15	COSMOS ⁴
Malaysia	1.94	103.38	Orchard	Dec 2014 – Nov 2015 (12)	88	0-5	TDR ¹⁵
Panama (1)	9.16	-79.84	Evergreen Broadleaf Forest	Jul 2012 – Nov 2017 (65)	330	0-10	TDR ¹⁶
Panama (2)	9.21	-79.75	Evergreen Broadleaf Forest	Jul 2015 – Dec 2017 (30)	203	0-10	EF ¹⁷

¹ Data not necessarily temporally continuous for every location

² COSMOS = Cosmic Neutron Probe, ECFT = Eddy Covariance Flux Tower, EF = Electromagnetic Field, GPS = Global Positioning System, TDR = Time Domain Reflectometry

³ Comprised of two sites at these coordinates

⁴ Köhli et al., 2015

⁵ Beringer et al., 2011

⁶ Beringer et al., 2007

⁷ Beringer et al., 2013

⁸ Jardine et al., 2019

⁹ Goulden et al., 2004

¹⁰ Wu et al., 2016

¹¹ Larson et al., 2008

¹² Ochoa-Sánchez et al., 2018

¹³ Bonal et al., 2008; and see Acknowledgements

¹⁴ Meijide et al., 2018; and see Acknowledgements

¹⁵ Kang et al., 2016

¹⁶ Rubio and Detto, 2017

¹⁷ Bretfeld et al., 2018



Table 2: Mean ranking of proposed cluster groups across OND and JFM during three super El Niños for tests used in R package NbClust (version 3.0). Low scores denote highest ranking.

Test	4	5	6	7	8	9	10
KL ¹	2.83	4.33	3.83	4.17	5.17	3.50	4.17
CH ²	5.00	6.17	5.33	3.50	3.50	1.83	2.67
CCC ³	3.33	4.33	3.67	4.33	4.50	3.83	4.00
Cindex ⁴	1.50	2.00	2.83	3.83	5.33	6.17	6.33
DB ⁵	4.33	2.00	2.83	2.83	4.33	6.17	5.50
Silhouette ⁶	2.67	4.50	5.83	4.17	4.00	2.83	3.83
Ratkowsky ⁷	1.00	2.00	3.00	4.00	5.00	6.00	7.00
Ptbiserial ⁸	1.33	1.67	3.00	4.17	4.83	6.00	7.00
McClain ⁹	7.00	6.00	4.83	4.17	2.83	2.00	1.17
Dunn ¹⁰	3.50	4.67	2.67	3.00	4.50	3.17	4.67
SDindex ¹¹	7.00	5.33	4.33	4.00	3.50	2.83	1.00
SDbw ¹²	1.00	2.00	3.17	4.00	4.83	6.17	6.83
Mean	3.38	3.75	3.78	3.85	4.36	4.21	4.51

¹ Krzanowski and Lai, 1988

² Calinski and Harabasz, 1974

³ Sarle, 1983

⁴ Hubert and Levin, 1976

⁵ Davies and Bouldin, 1979

⁶ Rousseeuw, 1987

⁷ Ratowsky and Lance, 1978

⁸ Milligan 1980; Milligan 1981

⁹ McClain and Rao, 1975

¹⁰ Dunn, 1974

¹¹ Halkidi et al., 2000

¹² Halkidi and Vazirgiannis, 2001



Table 3: Mean and standard deviation of October to December (OND) and January to March (JFM) change in the GLDAS soil moisture for clustered regions in the humid tropics. Statistics computed using OND and JFM GLDAS soil moisture anomalies during El Niño years 1982-83, 1997-98, and 2015-16 relative to the 1979-2016 mean.

Region ¹	Season	1982-83, 1997-98, 2015-16 Mean Change ± Standard Deviation
Cluster-1	OND	-0.05 ±0.02, 0.01 ±0.02, 0.07 ±0.02
Cluster-2	OND	-0.12 ±0.02, -0.06 ±0.02, -0.15 ±0.02
Cluster-3	OND	0.06 ±0.02, 0.10 ±0.02, 0.04±0.03
Cluster-4	OND	0.01 ±0.02, 0.05 ±0.02, -0.01 ±0.02
Cluster-1	JFM	-0.07 ±0.02, -0.03 ±0.02, -0.06 ±0.02
Cluster-2	JFM	-0.12 ±0.02, -0.10 ±0.02, -0.12 ±0.03
Cluster-3	JFM	0.09 ±0.02, 0.12 ±0.02, 0.08 ±0.02
Cluster-4	JFM	0.01 ±0.02, 0.06 ±0.02, 0.02 ±0.01



Table 4: Mean and standard deviation of October to December (OND) and January to March (JFM) change in soil moisture to precipitation ratio for the same regions shown in Table 3. Statistics computed using OND and JFM GLDAS soil moisture anomalies during El Niño years 1982-83, 1997-98, and 2015-16 relative to the 1979-2016 mean.

Region ¹	Season	1982-83, 1997-98, 2015-16 Mean Change ± Standard Deviation
Cluster-1	OND	0.20 ±6.77, -0.01 ±3.11, 4.72 ±53.07
Cluster-2	OND	-0.15 ±6.42, 0.47 ±12.16, 1.40 ±0.53
Cluster-3	OND	0.01 ±6.38, 3.33 ±47.90, 0.26 ±6.40
Cluster-4	OND	-0.01 ±6.71, 12.35 ±284.91, -1.62 ±130.82
Cluster-1	JFM	1.38 ±4.26, 0.47 ±0.95, 29.67 ±1042.43
Cluster-2	JFM	1.10 ±0.20, 0.99 ±0.21, 1.33 ±0.86
Cluster-3	JFM	1.18 ±1.28, 1.91 ±1.88, 0.92 ±0.37
Cluster-4	JFM	0.64 ±22.22, -2.29 ±79.17, 0.72 ±7.77



Table 5: Mean and standard deviation of October to December (OND) and January to March (JFM) change in soil moisture to evapotranspiration ratio for the same regions shown in Table 3. Statistics computed using OND and JFM GLDAS soil moisture anomalies during El Niño years 1982-83, 1997-98, and 2015-16 relative to the 1979-2016 mean.

Region ¹	Season	1982-83, 1997-98, 2015-16 Mean Change ± Standard Deviation
Cluster-1	OND	0.12 ±72.81, -0.21 ±1.12, 1.98 ±24.52
Cluster-2	OND	4.45 ±69.16, 0.47 ±1.86, 0.42 ±5.76
Cluster-3	OND	-0.21 ±75.51, 0.54 ±23.03, 0.53 ±15.53
Cluster-4	OND	0.36 ±54.18, -1.13 ±5.46, 4.88 ±135.52
Cluster-1	JFM	0.63 ±7.48, -0.82 ±24.18, 1.82 ±28.88
Cluster-2	JFM	0.34 ±16.37, 0.99 ±7.27, 1.87 ±22.99
Cluster-3	JFM	0.72 ±2.86, 20.12 ±398.90, 0.67 ±1.89
Cluster-4	JFM	-0.74 ±8.60, -5.71 ±133.99, 0.34 ±3.39



Table 6: Mean and standard deviation of 1979-2016 GLDAS soil moisture correlation with the Niño3.4 index for the same regions shown in Table 3.

Region ¹	Season	Mean Correlation ± Standard Deviation
Cluster-1	OND	-0.07 ±0.10
Cluster-2	OND	-0.12 ±0.13
Cluster-3	OND	-0.06 ±0.10
Cluster-4	OND	-0.06 ±0.10
Cluster-1	JFM	-0.06 ±0.07
Cluster-2	JFM	-0.09 ±0.07
Cluster-3	JFM	0.05 ±0.06
Cluster-4	JFM	0.00 ±0.08

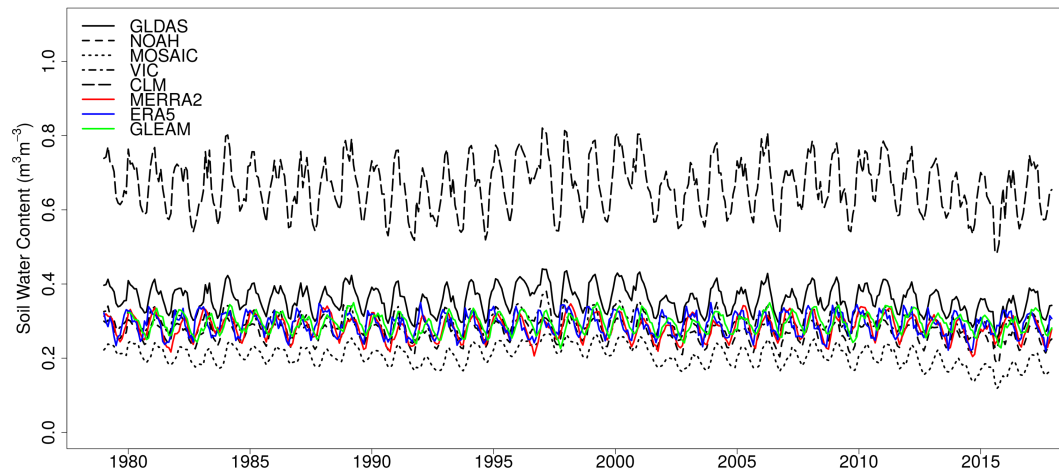


Figure 1: 1979-2017 monthly time series of mean soil moisture across all in-situ data locations shown in Table 1 for multiple data products including the GLDAS multi-model mean (black, solid), MERRA2 (red, solid), ERA5 (blue, solid), and GLEAM (green, solid), as well as the individual land surface models that make up GLDAS: NOAH (black, short dash), MOSAIC (black, dot), VIC (black, dash dot) and CLM (black, long dash). Note that the GLEAM time series starts from 1980.

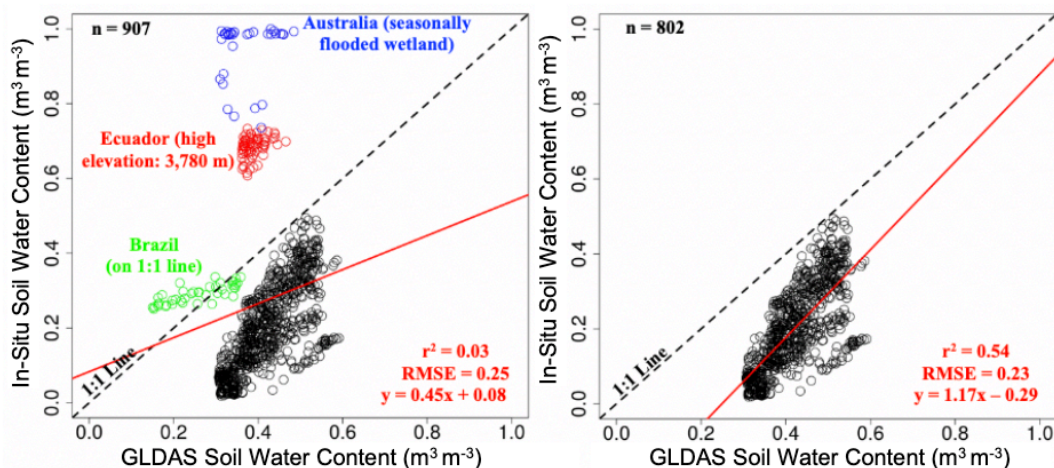


Figure 2: In-situ soil moisture vs. GLDAS soil moisture during October to December (OND) and January to March (JFM) for El Niño years 1982-83, 1997-98, and 2015-16. Each circle corresponds to one in-situ data point in space and time. The left panel includes data from all 18 sites shown in Table 1, with data from Australia, Ecuador, and Brazil highlighted in blue, red, and green, respectively. The right panel shows the same information with the Ecuador, Australia, and Brazil site data removed. The blue dashed line and red solid line represent the 1:1 line and the regression line, respectively.

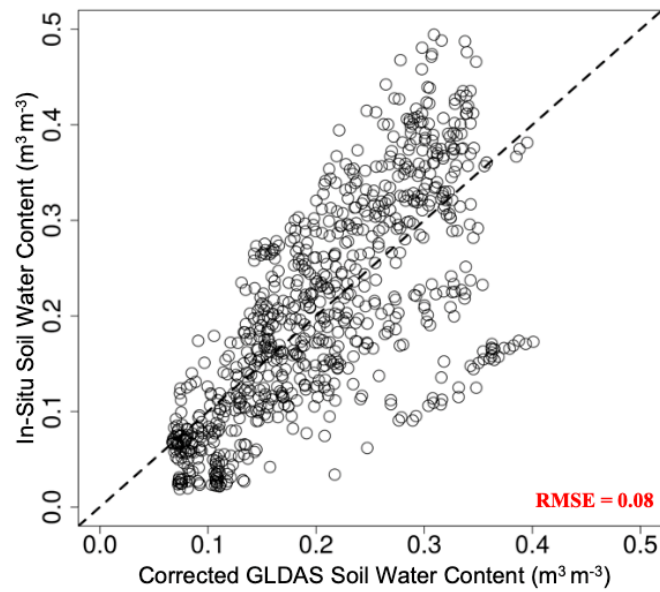


Figure 3: Bias-corrected soil moisture estimates from GLDAS relative to in-situ soil moisture observations for all sites with the mean RMSE shown in red.

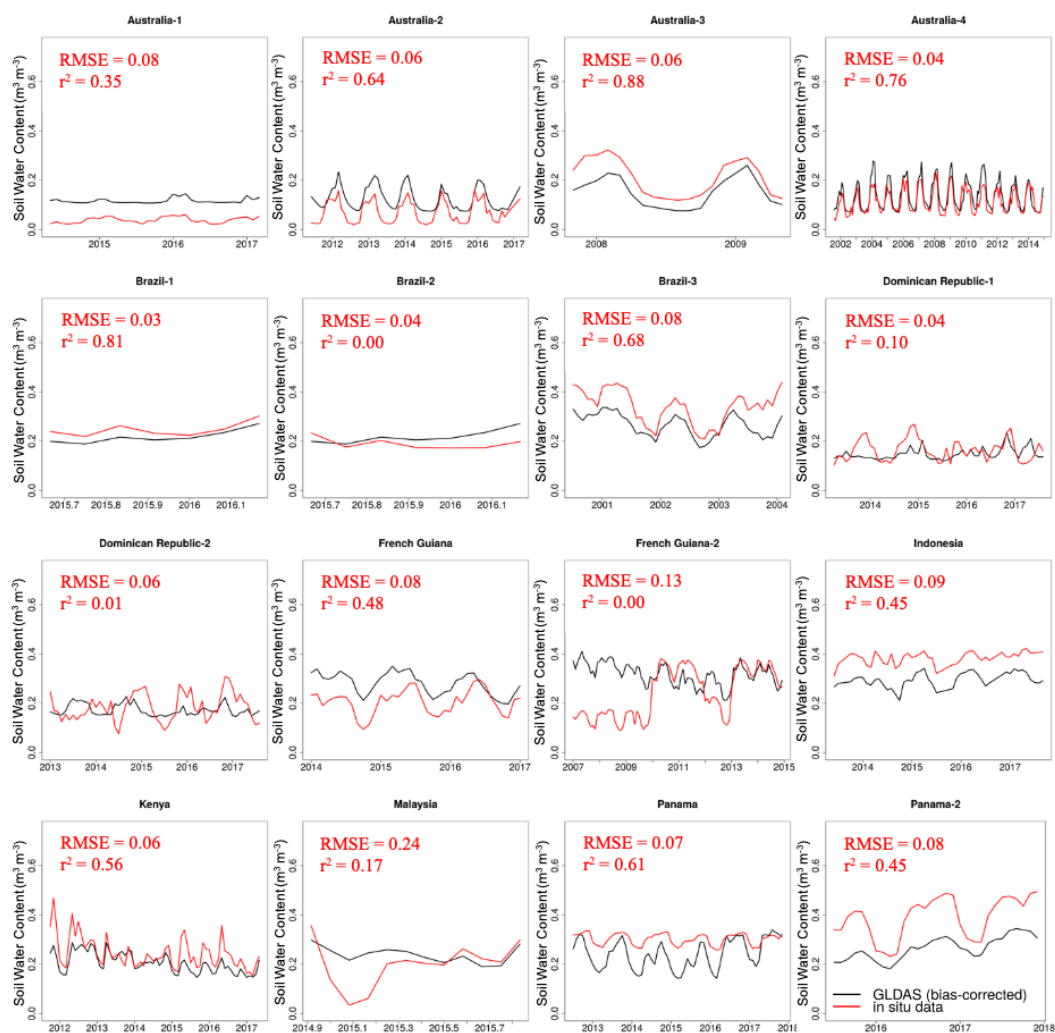


Figure 4: Bias-corrected estimate from GLDAS (black line) and in-situ observation (red line) of soil water content for 16 individual locations in the humid tropics. RMSE and r^2 coefficient of determination for each location are also shown.

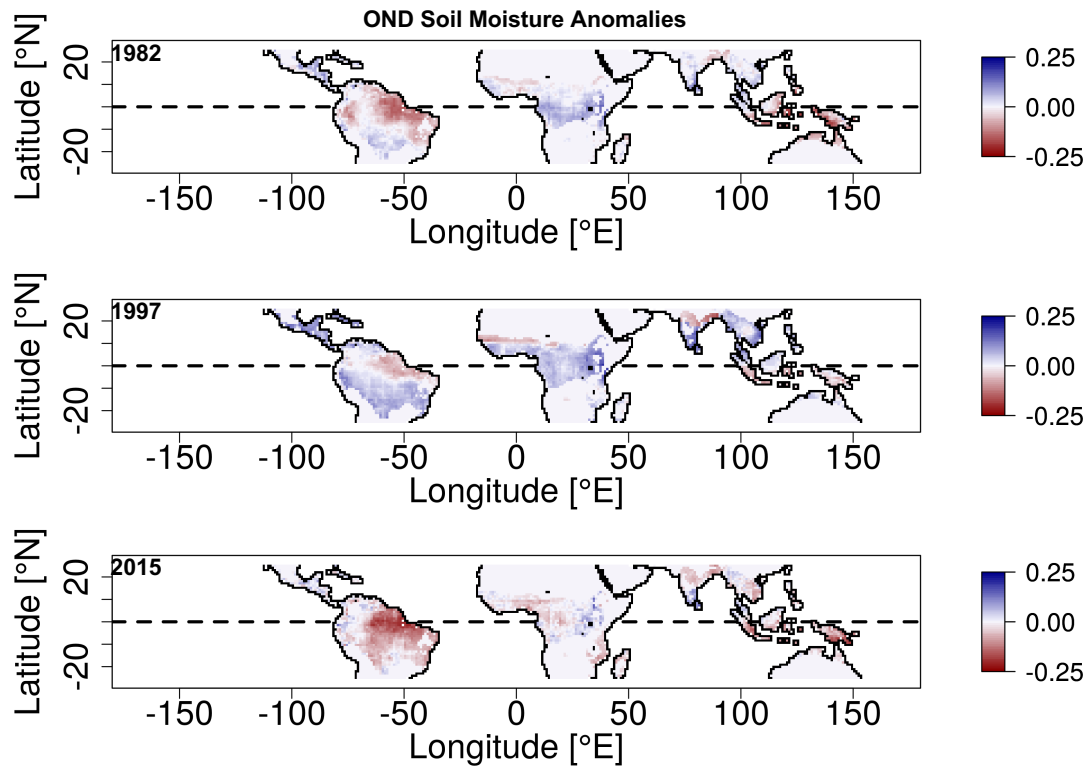


Figure 5a: October to December (OND) change in GLDAS soil moisture anomalies during the super El Niño years 1982 (top), 1997 (middle), and 2015 (bottom) relative to the previous years. Anomalies relative to 1979-2016 period.

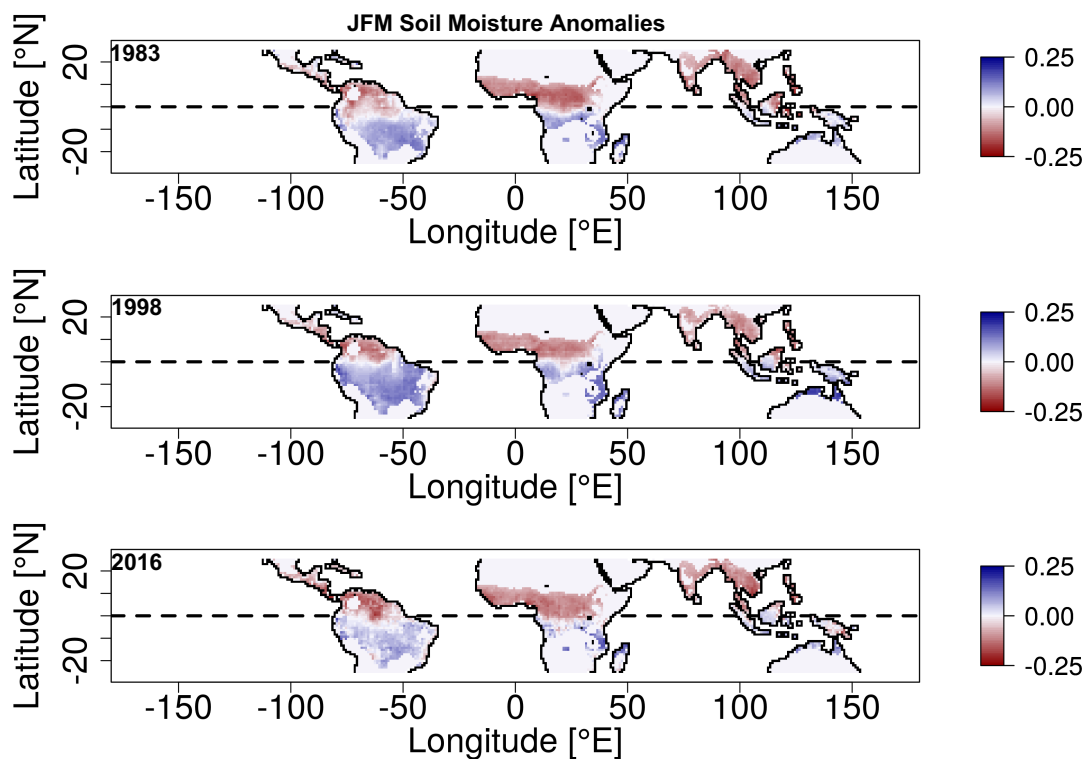


Figure 5b: Same as Figure 5a, but for January to March (JFM) in 1983 (top), 1998 (middle) and 2016 (bottom).

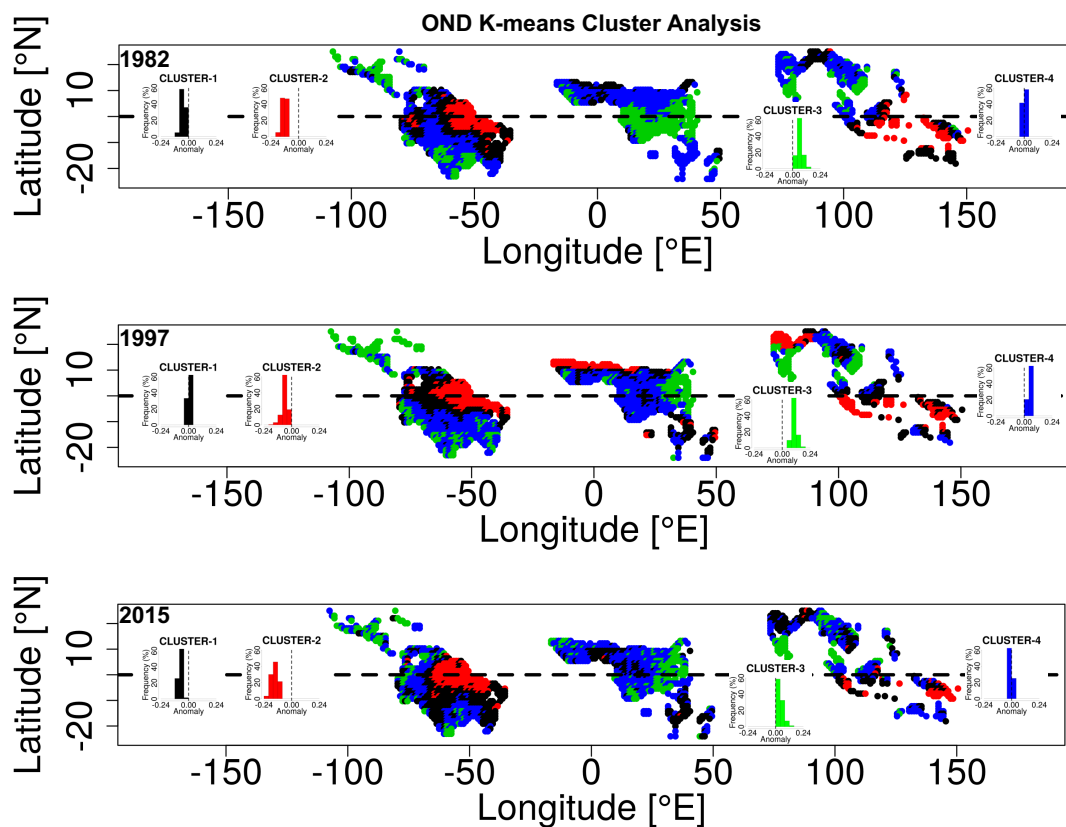


Figure 6a: K-means cluster analysis results for October to December (OND) for 1982 (top), 1997 (middle) and 2015 (bottom). Corresponding histograms of soil moisture anomalies for each of the four clusters also shown. Anomalies relative to 1979-2016 period.

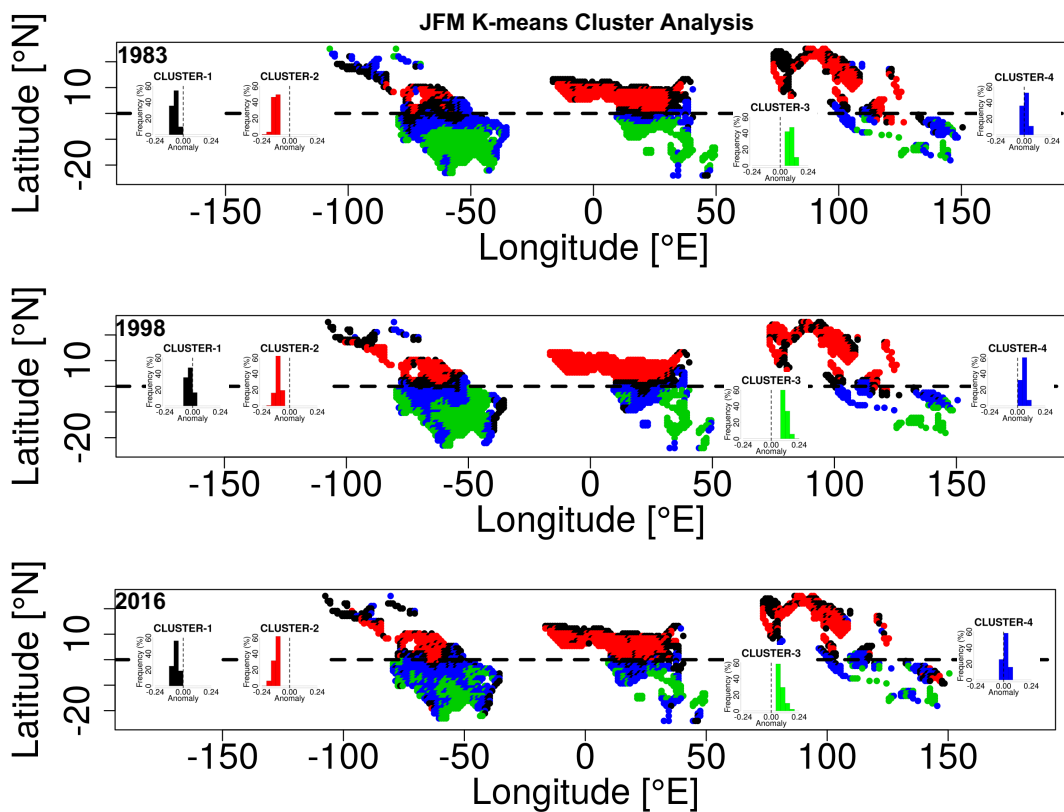


Figure 6b: Same as Figure 6a, but for January to March (JFM) in 1983 (top), 1998 (middle) and 2016 (bottom).

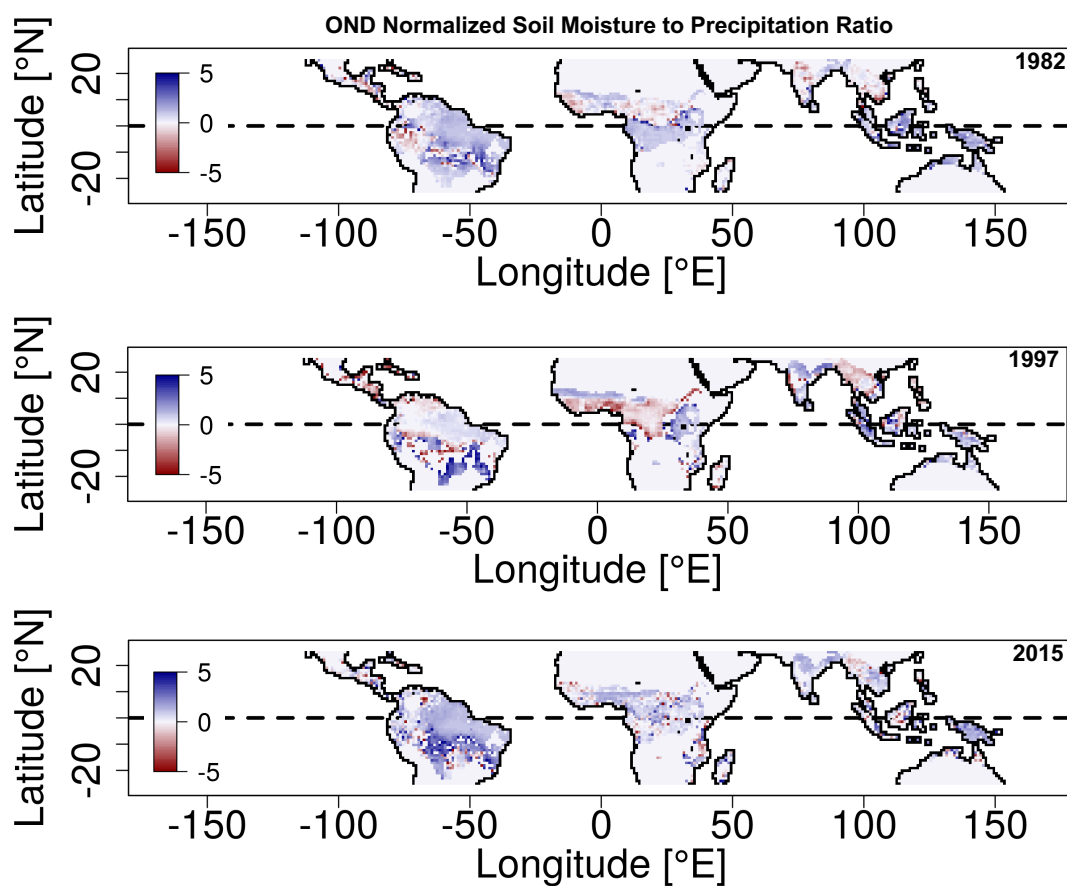


Figure 7a: Ratio of GLDAS soil moisture to precipitation change computed using October to December (OND) anomalies during El Niño years 1982-83, 1997-98, and 2015-16 relative to previous years. Anomalies normalized by the mean relative to 1979-2016 period.

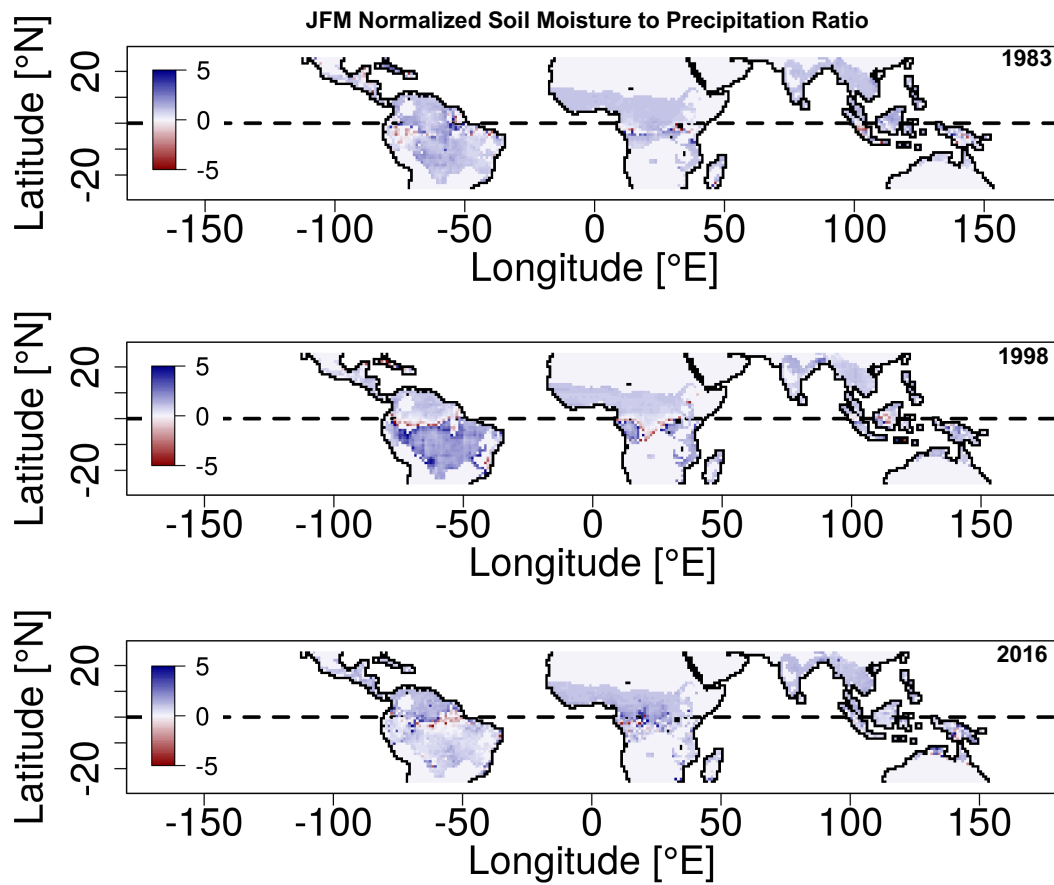


Figure 7b: Same as Figure 7a but for January to March in 1983 (top), 1998 (middle) and 2016 (bottom).

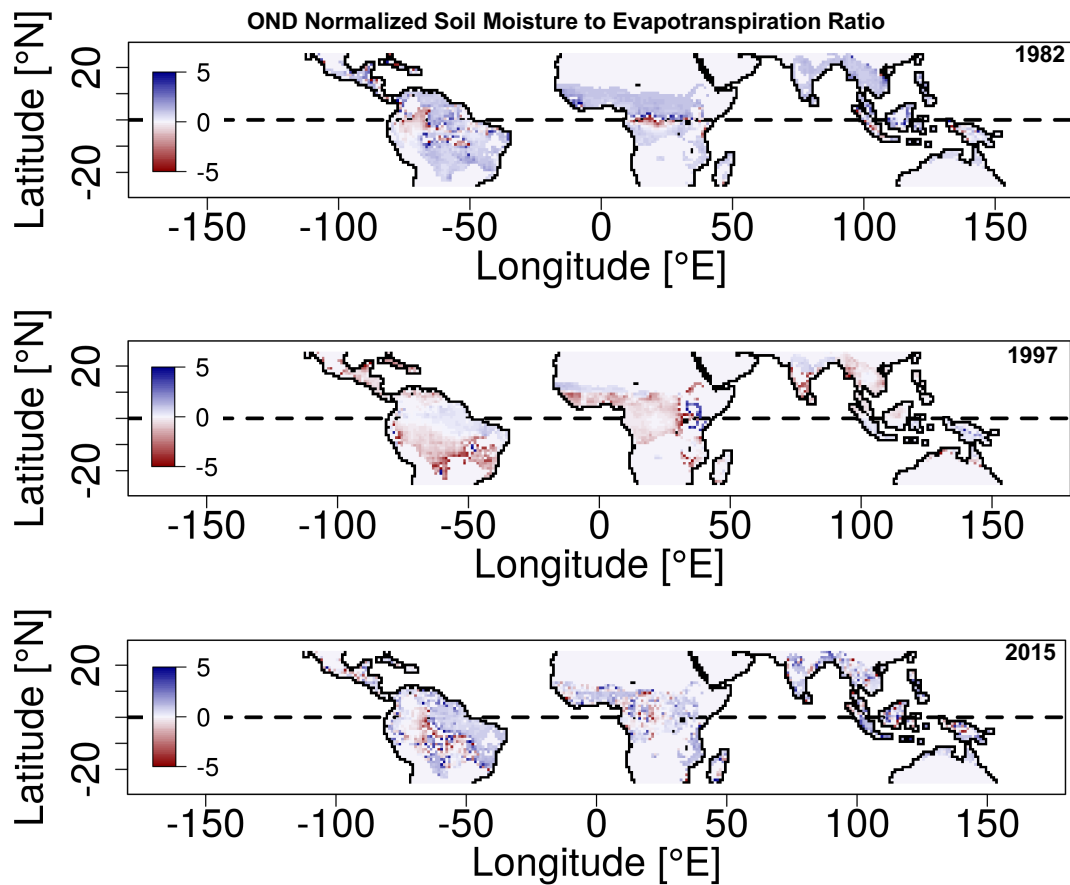


Figure 8a: Ratio of GLDAS soil moisture to evapotranspiration change computed using October to December (OND) anomalies during El Niño years 1982-83, 1997-98, and 2015-16 relative to previous years. Anomalies normalized by the mean relative to 1979-2016 period.

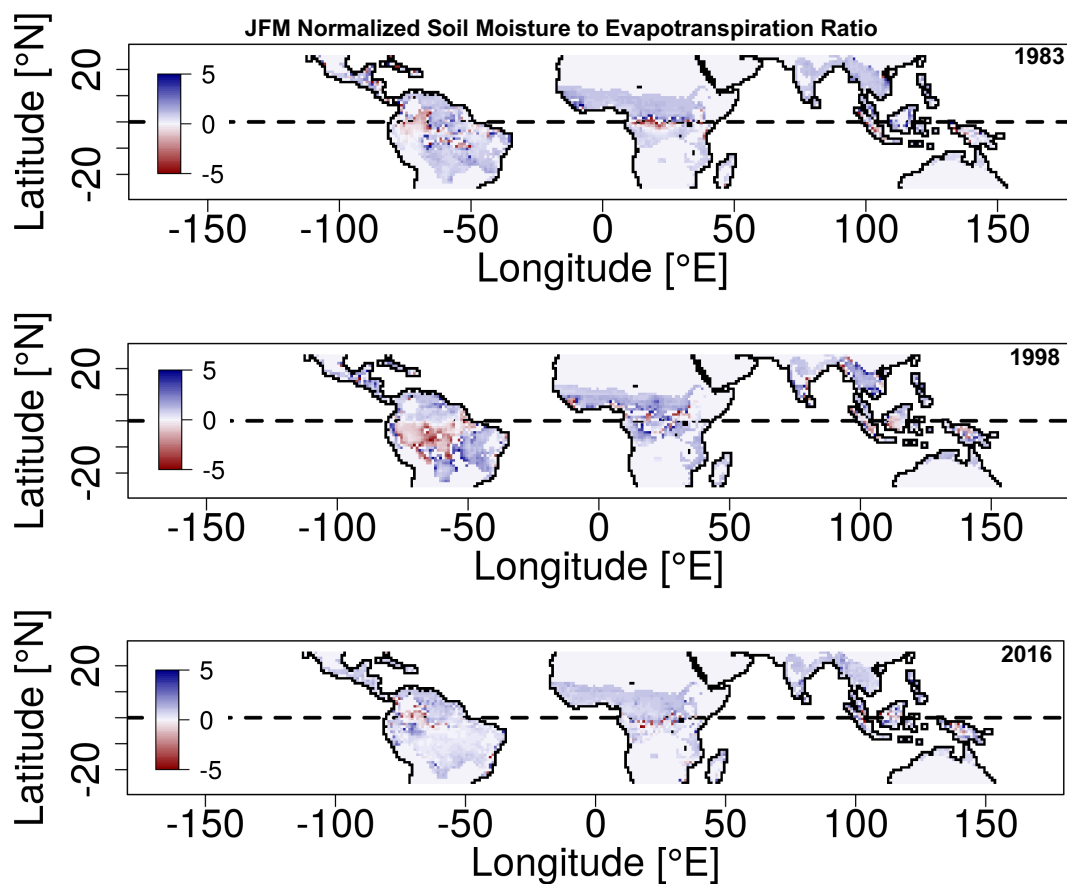


Figure 8b: Same as Figure 8a but for January to March in 1983 (top), 1998 (middle) and 2016 (bottom). Anomalies normalized by the mean relative to 1979-2016 period.

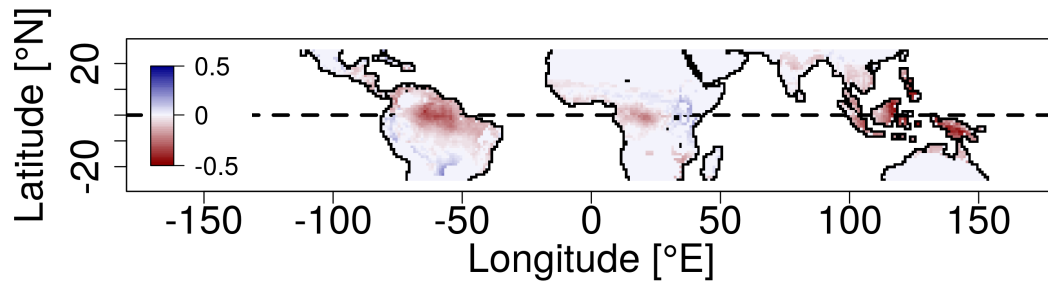


Figure 9: Pearson correlation coefficient between GLDAS soil moisture and NINO3.4 index from 1979 to 2016. Colors indicate regions where the mean correlation was negative (red) and positive (blue).

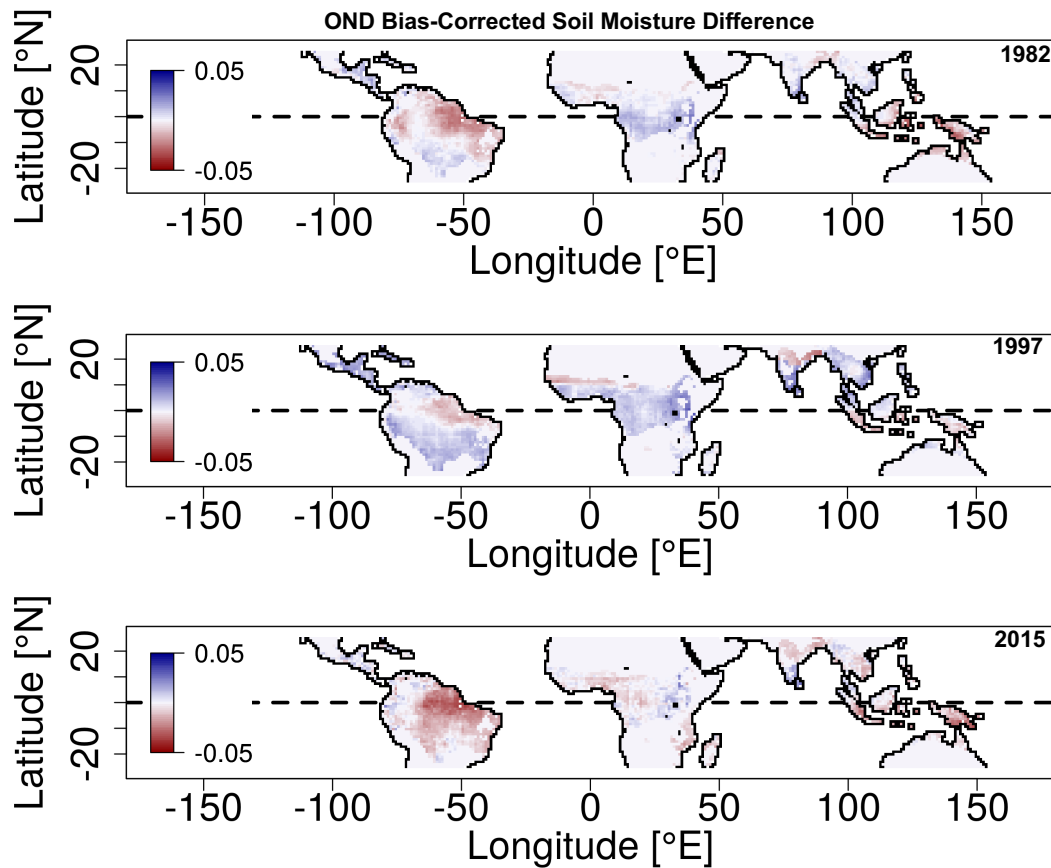


Figure 10a: Difference in October to December (OND) change in GLDAS soil moisture anomalies when bias correction is applied relative to no bias correction. Red pixels indicate regions that showed a decrease, while blue regions indicate regions that showed an increase with the addition of the bias correction. Plots shown for the super El Niño years 1982 (top), 1997 (middle), and 2015 (bottom).

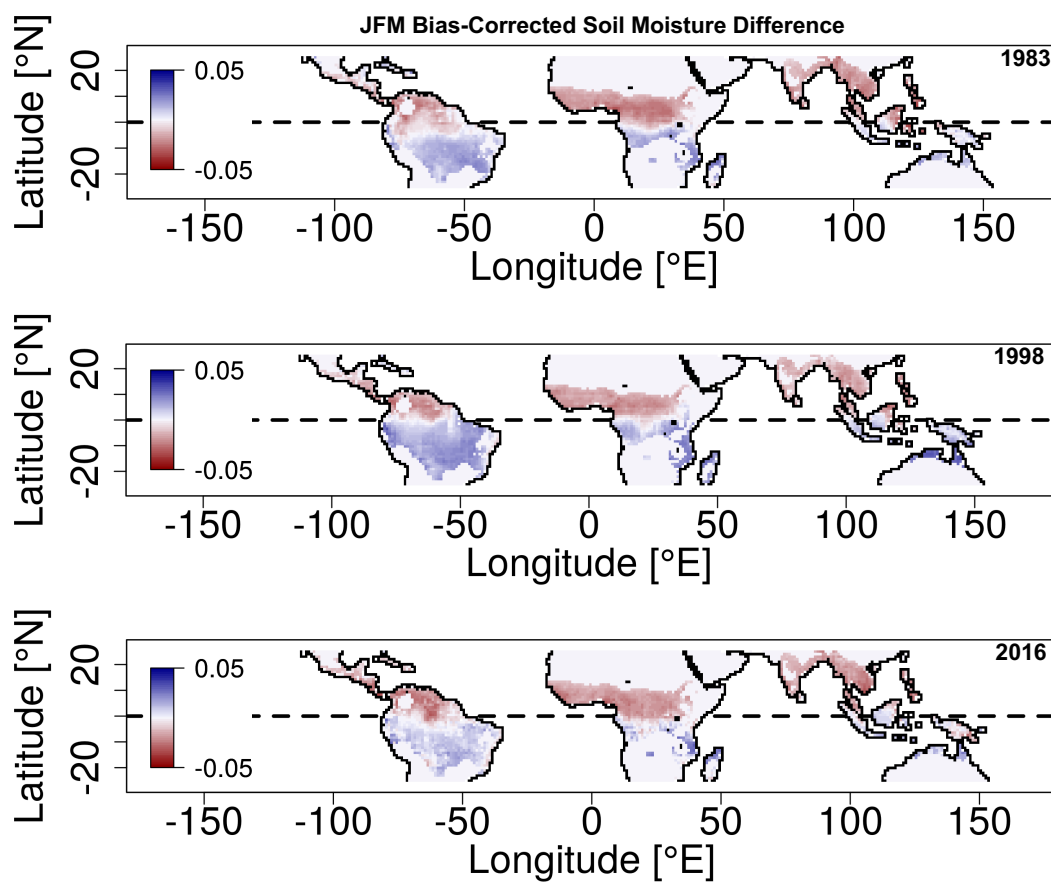


Figure 10b: Same as Figure 10a but for January to March (JFM) in 1983 (top), 1998 (middle) and 2016 (bottom).